Visualization of Physiological Responses by Observing 2D and 3D Liposome Dynamics

北陸先端科学技術大学院大学

中谷 祐将

博士論文

Visualization of Physiological Responses by Observing 2D and 3D Liposome Dynamics

中谷 祐将

主指導教員 高木 昌宏

北陸先端科学技術大学院大学

先端科学技術研究科 [マテリアルサイエンス]

令和 5 年 3 月

Abstract

【Background]

Cells sense the extracellular environment and initiate physiological responses to maintain homeostasis. Membrane receptors convert extracellular information into intracellular information by interacting with signal molecules. Dysregulation of signal transduction causes various diseases. Obesity and aging, which are abnormal states of lipid quality and quantity, are major risk factors for various diseases. Thus, it is possible that changes in lipidome affect the interaction between lipids and biological membrane properties and disturb signal transduction, eventually causing various diseases. However, the effect of lipid interactions and membrane properties on signal transduction is poorly understood. Lipid interactions and properties affect membrane dynamics. There are many kinds of membrane dynamics. We have classified these membrane dynamics into 2 types; 3D membrane dynamics (endocytosis, autophagy, exocytosis) and 2D membrane dynamics (lipid rafts). However, the biological membrane is not suitable for the analysis of lipid interaction because the components of the biological membrane are very complicated. Thus, in this thesis, we used biomimetic membranes (liposomes) because they can be prepared with simple compositions and are large enough to be observed by microscopy. We have studied 2D and 3D liposome dynamics. We have shown that liposomes cause deformation by adding surfactants and classified the 3D membrane dynamics depending on the strength of irritation. The evaluation method enables us to evaluate the irritancy of surfactants even when the irritancy of the surfactants is low. Liposomes can be changed their lipid compositions and phase-separated structures can be formed; liquid-ordered phase (Lo) rich in saturated lipids and cholesterol, liquid-disordered (Ld) phase rich in unsaturated lipids, and solid-ordered (So) phase rich in saturated lipids. This phase separation can be found in living cells. The So phase occurs in cholesterol (Chol)-poor endoplasmic reticulum (ER) and the Lo phase occurs in cholesterol-rich membranes such as cell membranes.

[Objective]

The purpose of this study was to visualize physiological responses using biomimetic membranes.

In chapter 2, we investigated the irritation of sodium cocoyl glutamate by an irritating evaluation system with 3D membrane dynamics. Furthermore, we examined the correlation between the irritancy evaluation system and the stinging test. In particular, the relationship between the carbon chain length of sodium glutamate and irritancy was examined. In chapter 3, we regarded So/Ld and Lo/Ld liposomes as ER membrane-model and raft model, respectively, and investigated the effect of two forms of vitamin E, α-Tocopherol(Toc) and α-Tocotrienol(Toc3), on amyloid β adsorption on these model membranes.

[Results]

In chapter 2, by observing membrane dynamics after adding amino acid surfactant to liposome solution, we found that comparing the irritancy of sodium cocoyl glutamate with that of its main component, sodium lauroyl glutamate, it was found in both liposome and stinging test that sodium lauroyl glutamate was the more irritating. The irritancy of sodium lauroyl glutamate was reduced by amphoteric surfactants. Furthermore, we established an evaluation system for Flip-Flop rate, which is important for membrane deformation. In chapter 3, we found that Toc and Toc3 do not affect the Lo/ Ld phase separation. DSC measurements suggested that affinity between Chol and VE (Toc and Toc3) is low, and VE is mainly incorporated into Ld phase in raft model membrane. Furthermore, DPH anisotropy measurement shows that VE increased the order of Ld phase. As the result, line tension of Lo/Ld phase boundary was decreased by adding VEs. Toc and Toc3 decreased the phase separation of So/Ld phase separation. DSC measurement using DPPC/VE binary system suggested that VE decreased the interaction between DPPCs. The effect was more strongly for Toc3 than Toc. Thus, the amount of Toc which is incorporated into So phase was larger than Toc3. We found that inhibition of So phase by Toc and Toc3 decreases amyloid β adsorption onto ER membrane model. Our experimental results show that changes in lipids interactions are closely related to physiological responses, and that visualization by 2D and 3D membrane dynamics can serve as a model system for various physiological responses. Furthermore, combined with superior image processing systems, we will be able to understand physiological responses in even greater detail.

[Keyword]

Liposome, Membrane deformation, Surfactant, Phase separation, Amyloid-β

Contents

Chapter 1
General Introduction

1-1 Signal transduction

Cells sense their extracellular environment and adapt to its changes by triggering physiological responses such as proliferation, cell death, and homeostasis control(Galluzzi et al., 2018; Schwarz and Blower, 2016; Villaseñor et al., 2015). These responses are initiated by the activation of receptors embedded in biological membranes. Activation of receptors is caused by the interaction with ligands and activated receptors convert extracellular information into intracellular. This series of pathways is called signal transduction. Abnormalities in signaling pathways cause a variety of diseases, thus, it is important to develop a better understanding of the regulation of these pathways.

It has been reported that the membrane environment influences the activity of ion channels(Wiggins and Phillips, 2004). In addition, the existence of signaling pathways initiated by membrane lipid components has been demonstrated(Funk, 2001). The role of biological membranes in signal transduction is thought to be important. However, little is known about it.

1-2 Biological membrane and lipid raft

Signal transduction is primarily mediated by proteins, which are localized in biological membranes. The biological membrane serves as a boundary between environments and assigns a specific role to each compartment. Biological membranes have lipid bilayers structure composed mainly of phospholipids, cholesterols, and membrane proteins (Fig. 1-1) (Jacquemyn et al., 2017; van Meer et al., 2008).

In 1972, G. L. Nicolson and S. J. Singer proposed a “fluid mosaic model” in which the components of the biological membrane diffuse freely across the membrane(Singer and Nicolson, 1972). In this model, biological membranes are simply considered scaffolds for membrane proteins that initiate signaling pathways. Recently it has been suggested that a relatively highly ordered lipid micro-domain forms on the plasma membrane. These regions are called “lipid raft” and is thought to be rich in saturated lipids and cholesterols(Fig. 1-2)(Rajendran and Simons, 2005; Simons and Ikonen, 1997). The lipid raft is considered insoluble in Triton X-100 due to its characteristic lipid composition(Parton and Simons, 1995; Schuck et al., 2003). When cells were treated with Triton X-100 and the insoluble fraction was obtained, various receptors were found to be present, such as glycosylphosphatidylinositol (GPI)-anchored proteins and epidermal growth factor receptor (EGFR)(Brown and Rose, 1992; Puri et al., 2005). Therefore, lipid raft is thought to accumulate these proteins and function as important platforms for signal transduction.

Recently, the relationship between membrane properties and physiological responses has become elucidated. It has become clear that changes in lipid composition and membrane properties affect various physiological responses such as cell differentiation,

protein transport, receptor activation, and effector protein recruitment(Capolupo et al., 2022; Fuentes et al., 2021; Schuhmacher et al., 2020; Sezgin et al., 2017). However, biological membranes are non-equilibrium systems that undergo constant metabolism and constantly change their composition. Furthermore, lipid rafts are thought to be small and disappear quickly. Therefore, the formation of rafts and their effects on physiological responses are difficult to elucidate.

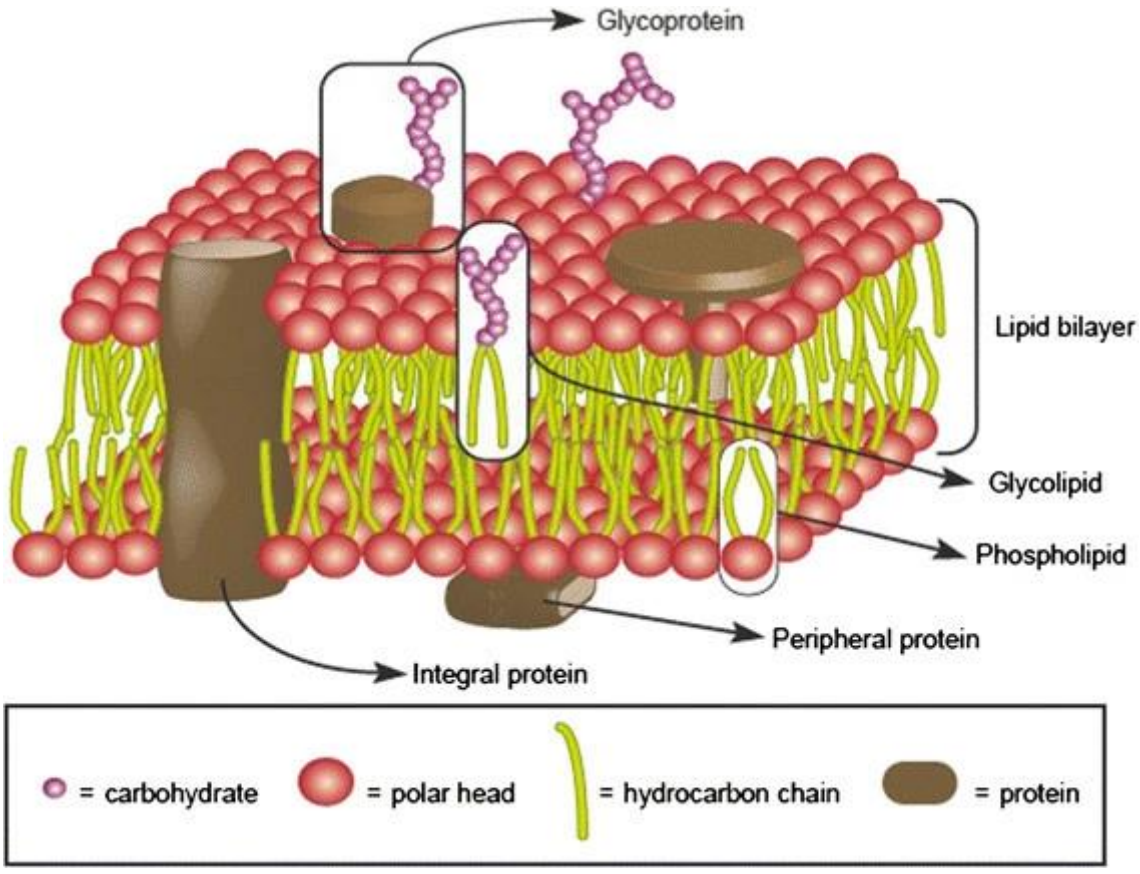

Fig. 1-1 Scheme of biological membrane(Lombard, 2014)

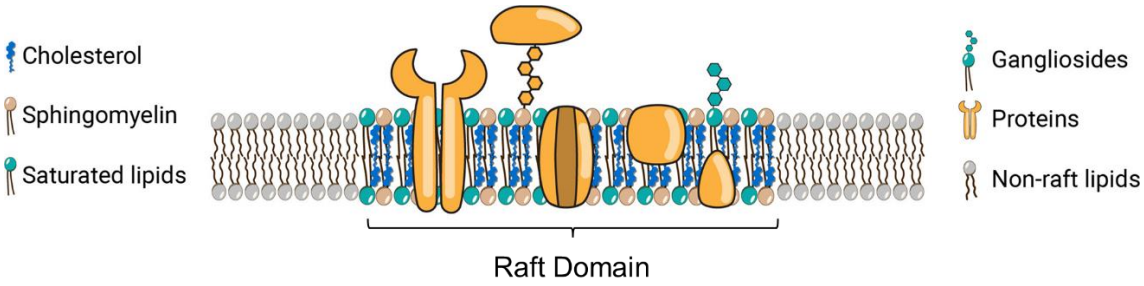

Fig. 1-2 Scheme of lipid raft(Nieto-Garai et al., 2022)

1-3 Cell membrane damage

Signal transduction occurs not only by proteins but also by lipid molecules(Bagga et al., 2003; Funk, 2001). Eicosanoids, produced from arachidonic acid, are a group of lipids that act as signaling molecules(Funk, 2001). The production of arachidonic acid has a pathway that proceeds with increased intracellular Ca^{2+} in the cytoplasm and originates in plasma membrane damage. Free fatty acids and plasma membrane-disrupting peptides are present extracellularly. These cell membrane-damaging molecules perforate the plasma membrane. The plasma membrane forms a concentration gradient of biomolecules. Because the biological membrane is a hydrophobic environment, ionic molecules cannot pass through the biological membrane. When this concentration gradient is disrupted by disruption of the biological membrane, various physiological responses occur. One of the molecules that trigger these physiological responses is Ca^{2+}. Ca^{2+} are kept at higher concentrations outside the cell than inside the cell. Therefore, they enter the cytoplasm during membrane pore formation. If the membrane pore is too large due to membrane damage, too many Ca2+ flow in and the cell undergoes necrosis, a non-programmed cell death. Necrosis cells release cell contents into the surrounding area, activating the innate immune system, including PPARs, and causing inflammation. When membrane pores are small (~100nm), influx Ca^{2+}-dependent membrane repair occurs(Jimenez et al., 2014; Zhen et al., 2021). On the other hand, Ca^{2+} trigger the arachidonic cascade. The influx of Ca^{2+} is taken up by calmodulin and changes the structure of calmodulin (Fig. 1-3). It then activates phospholipase A2, which degrades plasma membrane phospholipids and produces arachidonic acid.

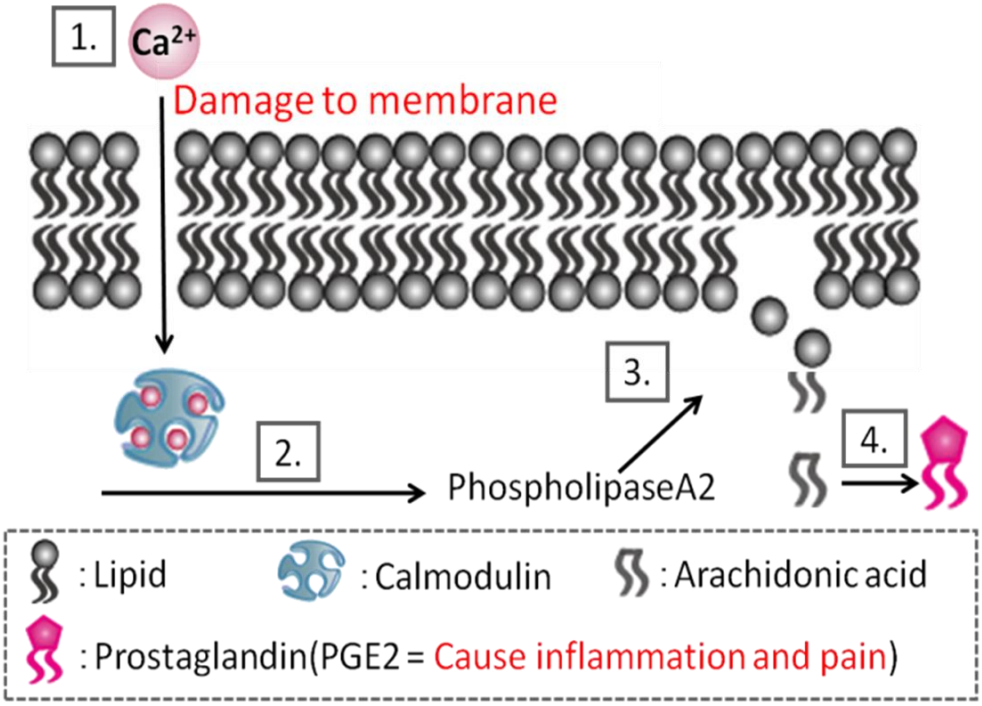

Fig. 1-3 Scheme of the mechanism of skin irritation

1-4 Endoplasmic Reticulum stress

ER is the largest membrane-bound organelle in the cell. ER is responsible for protein and lipid synthesis and is important for cell function(Schwarz and Blower, 2016). Furthermore, ER is responsible for controlling homeostasis in the quality and quantity of proteins and lipids, called proteostasis and homeoviscuous, respectively(Radanović and Ernst, 2021). Disruption of these homeostases is called ER stress. Under ER stress, cells initiate a variety of adaptive responses called unfolding protein responses (UPR) (Fig. 1-4)(Adams et al., 2019; Almanza et al., 2019; Sano and Reed, 2013).

The correct three-dimensional conformation of proteins is necessary for their proper function, and secretory and membrane proteins are properly folded in the ER prior to localization to their target compartments. The ER contains a variety of proteins involved in folding, including folding-mediating chaperones and folding-checking mechanisms, which control folding quality. Misfolding proteins are formed depending on the state of the cell. Misfolding proteins are cytotoxic, and cells have an evasive response. As a starting point for the avoidance response, the ER membrane contains three sensor proteins that are activated in the presence of misfolded proteins. The sensor proteins are Inositol requiring enzyme 1 (IRE1), PKR-like endoplasmic reticulum kinase (PERK), and activating transcription factor 6 (ATF6). Downstream of these sensor proteins are pathways involved in chaperone synthesis, degradation pathways (ubiquitin-proteasome pathway), and cell death, which can reduce ER stress or cause cell death in response to excessive stress.

ER stress has been shown to be activated not only by misfolded proteins but also by lipids(Ariyama et al., 2010; Halbleib et al., 2017; Piccolis et al., 2019; Promlek et al.,

2011; Radanović and Ernst, 2021; Thibault et al., 2012; Volmer et al., 2013). Previous studies showed that ER membrane abnormalities such as increased phosphatidyl ethanolamine/phosphatidylcholine, increased saturated lipids, and inositol depletion cause activation of IRE1 and PERK. in a denatured protein-independent manner.

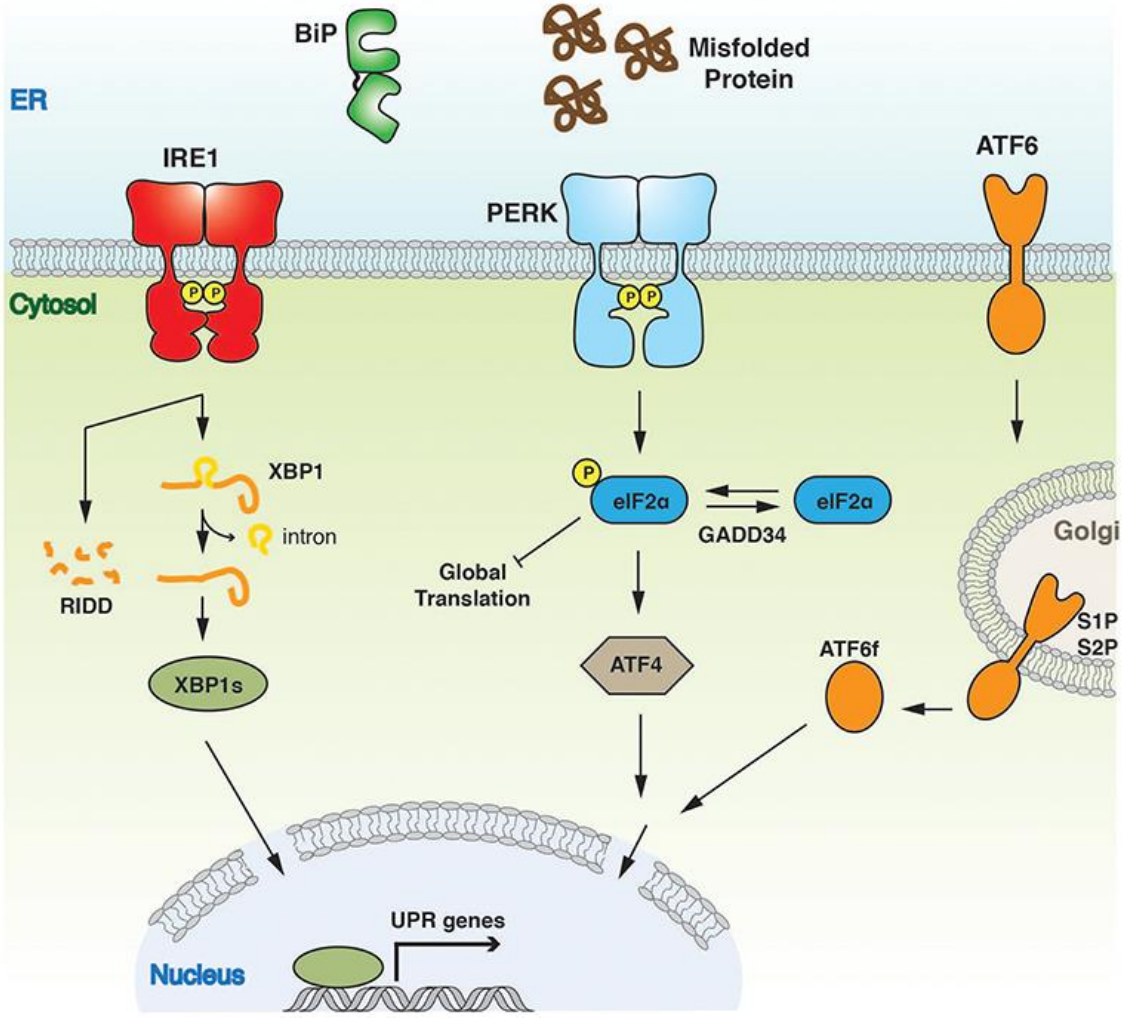

Fig. 1-4 Scheme of The UPR pathway initiated by a sensor protein embedded in the ERmembrane(Adams et al., 2019).

1-5 Liposome

Biological membranes contain a lot of kind of lipids. Furthermore, there are numerous membrane proteins embedded in biological membranes and biological membranes interact with cytoskeletal proteins at the surface(Sezgin et al., 2017). In addition to the complexity of the membrane components, biological membranes are non-equilibrium environmentwhose components and external environment are constantly changing(Fanning et al., 2019; Shen et al., 2017). Thus, it is difficult to analyze lipid interactions in such a complex environment. For these reasons, liposomes are used as a biological membrane mimetic system to make intermolecular interactions clearer. Liposomes are composed mainly of phospholipids and have a lipid bilayer structure same as biological membranes (Fig. 1-5). The lipid composition of liposomes can be freely selected. We can mimic not only plasma membrane but also membrane bound organelle, which has unique lipid component(Jacquemyn et al., 2017; van Meer et al., 2008). This ease of handling liposomes makes it possible to analyze the effect of hydrophobic molecules on membrane properties(Ko Sugahara et al., 2017; Shimokawa et al., 2017; Wongsirojkul et al., 2022). Previously, using liposomes, membrane lipid interactions have been analyzed under various environmental conditions with temperature, osmotic pressure, and pH as variables(Guo et al., 2021; Ko Sugahara et al., 2017; Wongsirojkul et al., 2020).

The phospholipids that constitute liposomes are amphiphilic, so when phospholipids are dissolved in a polar solvent, bilayer structures are formed, with the hydrophilic groups moving toward the solvent and the hydrophobic groups facing each other. Various methods have been developed for liposome preparation, such as natural swelling method, solvent dispersion method, and extruder methods, etc.(Akbarzadeh et al., 2013).

Liposomes larger than 1 μm are called giant unilamellar vesicles (GUVs), liposomes smaller than 1 μm are called large unilamellar vesicles (LUVs), and liposomes smaller than 100 nm are called small unilamellar vesicles (SUVs)(Fig. 1-6)(van Swaay and deMello, 2013).

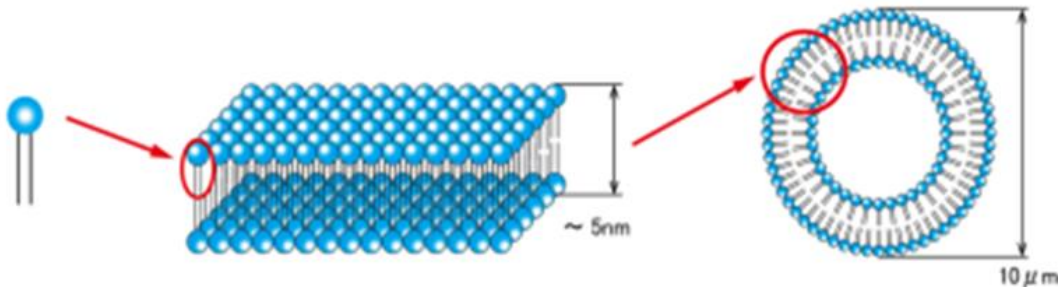

Fig. 1-5 The structure of liposomes.

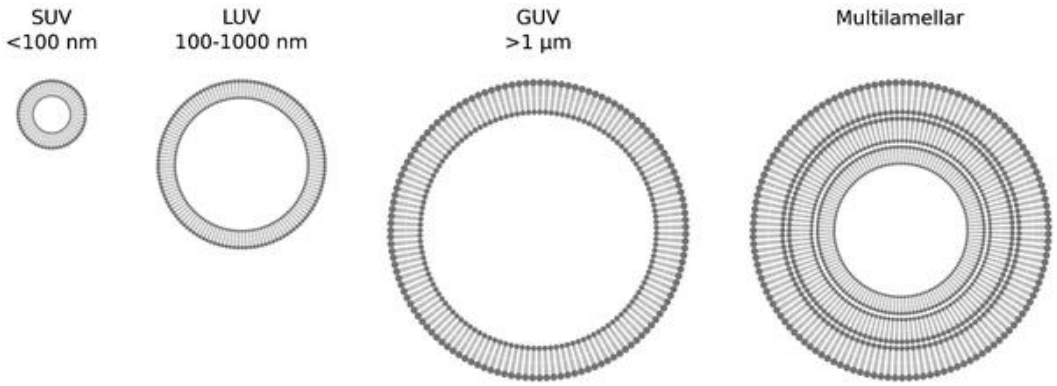

Fig. 1-6 Liposome classification(van Swaay and deMello, 2013).

1-6 Membrane dynamics

As mentioned above, cells are exposed to a variety of factors that can damage cell membranes. We have attempted to mimic the membrane damage induced by surfactant using GUVs(Hamada et al., 2012). We found that membrane deformation caused by surfactants varies depending on the stimulus intensity of the surfactant (Fig. 1-7). This classification method can be an alternative stimulus evaluation test to animal experiments. It can classify weakly and no irritation, which has been difficult to evaluate in conventional animal and live cell experiments(Wilson et al., 2015).

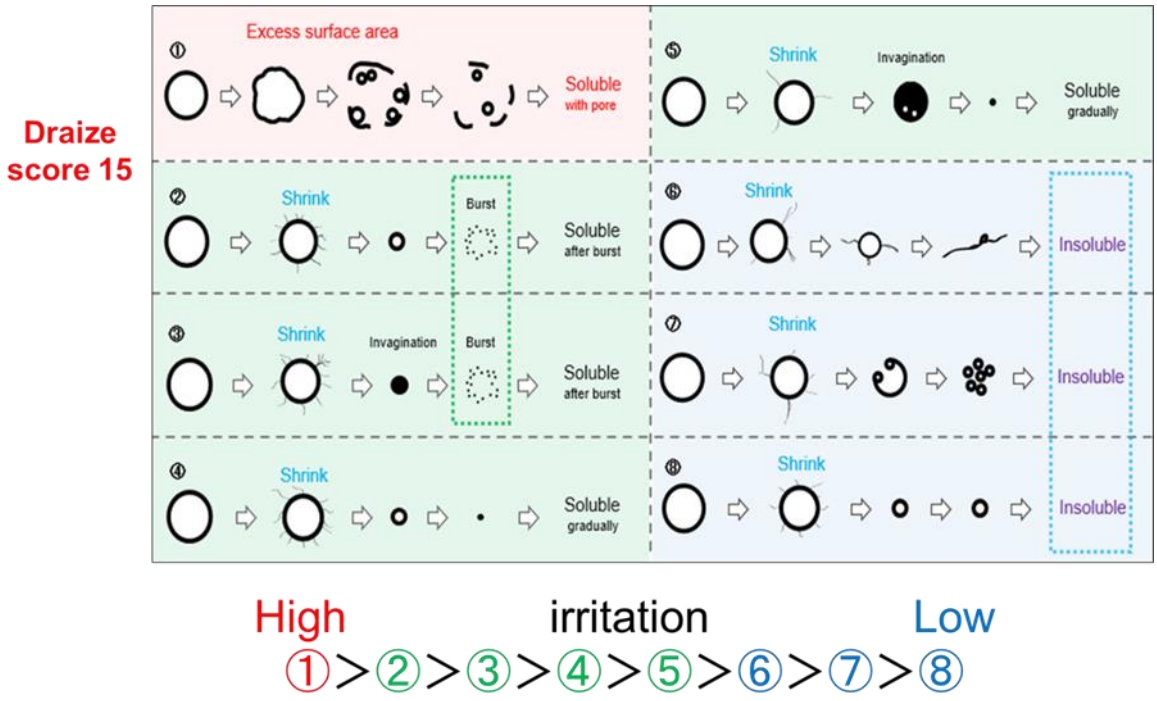

Fig. 1-7 Membrane dynamics induced by surfactants

・Dynamics①

The addition of surfactant causes the spherical liposomes to fluctuate. The membrane intrusion then occurs, and the liposomes eventually solubilize.

・Dynamics②

The addition of surfactant shrank liposomes while maintaining their spherical shape. The liposomes, then, burst and eventually solubilize.

・Dynamics③

The addition of surfactant shrank liposomes while fluctuating their spherical shape. The liposomes, then, burst and eventually solubilizes.

・Dynamics④

The addition of surfactant shrank liposomes, then eventually solubilize them.

・Dynamics⑤

The addition of surfactant shrank liposomes, then membrane intrusions and fluctuations occur. The liposomes eventually solubilize.

・Dynamics⑥

The addition of surfactant shrank liposomes, eventually the liposomes become a thread-like insoluble structure.

・Dynamics⑦

The addition of surfactant shrank liposomes and form membrane pores. Membrane fission then occurs, and finally, forming insoluble structures.

・Dynamics⑧

The addition of surfactant shrank liposomes and eventually they remain insoluble while maintaining their spherical structure.

1-7 Phase separation

Lipid rafts formed in cell membranes are thought to be important in signal transduction(Sezgin et al., 2017; Simons and Ikonen, 1997). The structures in which specific lipids accumulate are called phase-separated structures. Phase-separated structures have also been reported to form in the ER membrane(King et al., 2020; Shen et al., 2017; Tian et al., 2022). The ER membrane contains little cholesterol and forms a phase separated structure rich in saturated lipids (Jacquemyn et al., 2017; van Meer et al., 2008). This structure is also surfactant-resistant, but ER membrane proteins accumulate in this fraction is not known. Microscopic studies have shown that anchor proteins that form organelle contact regions accumulate in the phase-separated structures found in the ER membrane(King et al., 2020). Thus, the formation and degradation of phase-separated structures may have important functions in physiological reactions, and their elucidation is important.

Liposomes exhibit various phase-separated structures by changing their lipid composition (Fig. 1-8)(Veatch and Keller, 2005, 2003). These phase-separated structure can be reproduced with liposomes. In the three-component (saturated lipid/unsaturated lipid/cholesterol) , the coexistence of liquid-ordered (L_o) phase, rich in saturated lipid and cholesterol, and liquid-disoredered (L_d) phase, rich in unsaturated lipid, was found. In the binary-component (saturated lipid/unsaturated lipid), the coexistence of solid-ordered (S_o) phase, rich in saturated lipid, and liquid-disoredered (L_d) phase, rich in unsaturated lipid, is found. L_o and S_o phase can be regarded as models of lipid raft and phase separated structure found on ER membrane, respectively.

The occurrence of phase separation can be explained by the equation; free energy

F=U-TS (*U*= internal energy, *T*= temperature, *S*= entropy). At a given temperature, whether phase separation occurs or not is determined by which of *U*, which represents the interaction between lipids, and *S*, which represents entropy, is dominant. Lipid molecules behave in such a way that the free energy *F* is lower. If *U* is dominant, phase separation occurs, and if *S* is dominant, the lipids are uniformly dispersed in a mixed state. As can be seen from the free energy equation, the entropy term is proportional to temperature, so the entropy term becomes dominant at high temperatures. Therefore, when the temperature is higher than the phase separation disappearance temperature, *S* becomes dominant over *U*, resulting in a mixed state. At temperatures below the phase separation structure disappearance temperature, phase separation occurs because *U* predominates over *S*.

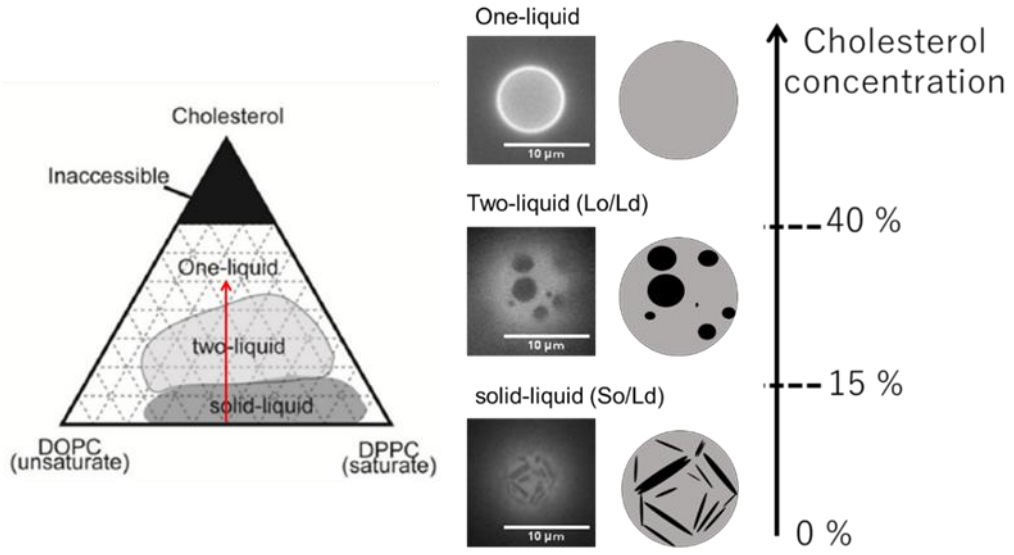

Fig. 1-8 Phase diagrams of ternary memrbanes (DOPC/DPPC/Chol) at 20℃ and images of phase separated GUVs(Veatch and Keller, 2003).

1-8 Research purpose

The biological membrane, which is the starting point of signal transduction, is important, and understanding its damage and phase separation is crucial to understanding signal tranduction. Therefore, the purpose of this study was to examine the relationship between physiological responses and membrane dynamics.

In Chapter 2, we focused on the relationship between 3D membrane dynamics and irritant property. The irritancy of amino acid surfactants was examined in a model system of cell membrane damage. In addition, the correlation between membrane test results and human puncture test results was examined. In addition, the rate of transbilayer movement of phospholipids (Flip-Flop) upon surfactant addition was examined in a LUV-based system to further reveal the relationship between irritancy and transbilayer movement of lipids.

In Chapter. 3, we focused on the relationship between 2D membrane dynamic (phase separation) and physiological responses. α-Tocopherol (Toc) and Tocotrienol (Toc3), forms of Vitamin E, have different functions in ER stress-induced neuronal cell death induced by 24SOHC(Kimura et al., 2018; Nakazawa et al., 2017; Urano et al., 2019). Toc and Toc3 differ only in the degree of unsaturation of their hydrocarbon chains. Therefore, we hypothesized that because of the difference in degree of unsaturation, they interact differently with the membrane, resulting in differential physiological responses. We reproduced in liposomes the phase-separated structures that are thought to form in cell and ER membranes and investigated the effects of Toc and Toc3 on phase separation. Toc and Toc3 lateral localization in phase separation is discussed by microscopic observations, thermal analysis, and fluorescence anisotropy studies. In

addition, the effects on membrane interactions with the misfolded protein Amyloid β (Aβ) was investigated and we discussed the relationship between Aβ membrane adsorption and the ER stress.

Chapter 2
Cell membrane damage model

2-1 Introduction

Cells are exposed to various kinds of irritating molecules. These molecules damage cells and induce inflammation. Surfactants are the one of the irritating molecules around us. Like phospholipid, surfactants have hydrophobic tails and hydrophilic head groups. Thus, they can interact with and solubilize biological membrane. The partially disruption of lipid bilayer structure causes the influx or efflux of biomolecules depending on their concentration gradients. The concentration of cytosolic Ca^{2+} is kept low compared with that of outer environment. Thus, damage to the cell membrane causes Ca^{2+} to flow into the cell(Burgos et al., 2011; Dalal et al., 2020). These Ca^{2+} bind to calmodulin and activate phospholipase A2 on the cell membrane(Moskowitz et al., 1985; Shimizu et al., 2008, p. 15). Phospholipase A2 esterifies phospholipids in the biological membrane, releasing arachidonic acid. Arachidonic acid is oxidized by cyclooxygenase to produce a variety of prostaglandins, which are causative agents of pain and inflammation. In particular, prostaglandin E2 and prostaglandin I2 enhance the inflammatory effects of plasma kinin by increasing vascular permeability. This sequence of pathways is called the arachidonic acid cascade, and damage to cell membranes is the starting point of the cascade(Jang et al., 2020; Meirer et al., 2014).

It is difficult to predict the irritancy of surfactants correctly, thus, their evaluation is important. The Draize test is one of the most common methods(Wilhelmus, 2001). The Draize test is a method of evaluating skin and eye irritation, in which surfactants are applied directly to rabbit eyes and the irritation score (Draize score) is determined. In the Draize test, the degree of irritation is determined visually by human observers and scored.

The results obtained from the Draize test are useful for the development of cosmetics and detergents. In particular, hypoallergenic surfactants with a Draize score of 0-15 (non-irritant/practically non-irritant/slightly irritating) are very difficult to subdivide because they are unlikely to cause obvious irritation in the Draize score.

In addition, the Draize test has been banned for animal welfare reasons since the test substance is administered directly into the eye of a live rabbit, and the OECD (Organization for Economic Cooperation and Development) has adopted two alternative methods for the Draize test: the bovine corneal enucleation test method and the chicken eye separation test method(Vinardell and Mitjans, 2008). These alternative methods correlate strongly with the Draize test and are considered valid alternatives. However, since these methods also use animals, they remain cruel tests on laboratory animals. Considering the above, there is a need to develop an alternative method to the Draize test that does not sacrifice animals and that can obtain high quantitative results even with hypoallergenic surfactants.

Since stimulation is induced by damage to cell membranes, we have been developing stimulation evaluation methods focusing on the interaction between phospholipids and surfactants. It is difficult to analyze the interaction of surfactants with cell membranes because they contain a variety of lipid and protein species. Therefore, we attempted to reproduce cell membrane damage using liposomes, which have a similar structure to the cell membrane and can be produced with a simple composition.

Our laboratory studies the correlation between surfactant stimulation and membrane dynamics in cell-sized liposomes(Hamada et al., 2012). And we have shown that there are membrane dynamics depending on the stimulation intensity (unpublished). Therefore, in this study, we will compare the results of liposome and stinging tests

developed by our laboratory using amino acid surfactants, which are hypoallergenic surfactants. In addition, the effect of surfactant on Flip-Flop rate is examined in a test system that measures the rate of lipid transbilayer movement.

2-2 Materials and Methods

2-2-1 Materials

Unsaturated lipid, 1,2-dioleoyl-*sn*-glycero-3-phosphocholine (DOPC), was purchased from Avanti Polar Lipid (Alabaster, USA). Llissamine™ rhodamine B 1,2-dihexadecanoyl-*sn*-glycero-3-phosphoethanolamine, triethylammonium salt (Rhodamine-DHPE) (λex = 560 nm, λem = 580 nm) was used to label Giant unilamellar vesicles (GUVs). Rhodamine-DHPE was purchased from Thermo Fisher (Waltham, USA). 1,2-Dipalmitoyl-sn-glycero-3-phosphoethanolamine-N-(7-nitro-2-1,3-benzoxadiazol-4-yl) (ammonium salt) (NBD-DPPE) was used to label LUVs. Triton X-100 was purchased from MP biochemicals (California, USA). Tween 20 was purchased from Santa Cruz Biotechnology (California, USA). Other surfactants were kindly provided by COTA CO., LTD.

DOPC

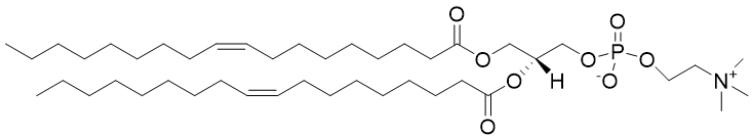

Rhodamine-DHPE

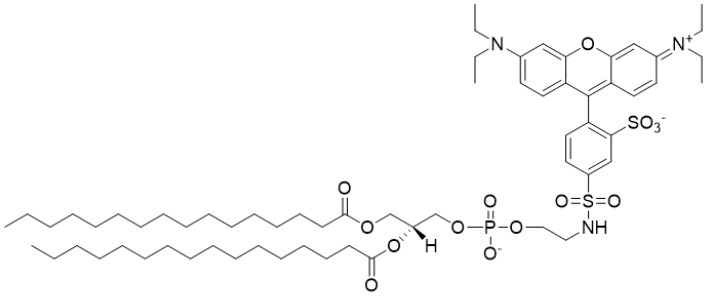

NBD-DPPE

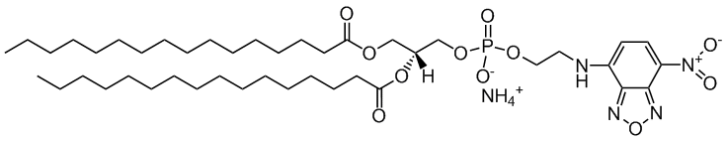

Fig. 2-1 Chemical structures of DOPC and fluorescence probes.

Sodium lauroyl gutamate

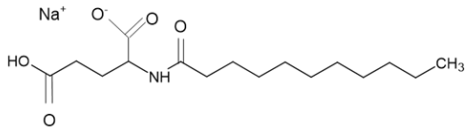

Cocamid propyl betaine

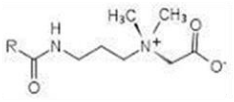

Lauramydopropyl betain

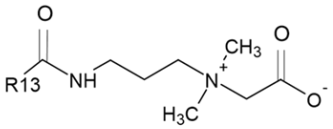

Tween 20

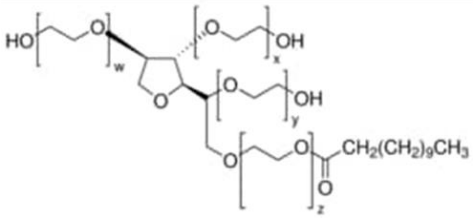

Fig. 2-2 Chemical structures of surfactants

2-2-2 GUV preparation for observation

In this study, GUVs were used for microscopy observation. GUVs were prepared by the natural swelling method (Fig. 2-3). DOPC was dissolved in chloroform/methanol (2: 1 v/v) to 2mM. Glucose was dissolved in chloroform was dissolved in methanol to 10mM. Rhodamine-DHPE was dissolved in chloroform to 0.1mM. Firstly, GUVs solution components were mixed with 20µl of DOPC, 12µl of glucose solution, and 8µl of Rhodamine-DHPE in an acetone-washed durham tube. Secondly, to make lipid films, the mixture was dried under a current of N_2 gas and leave them under a vacuum for more than 3hrs to volatilize the rest of the organic solvent completely. Finally, to form GUVs, the lipid film was added with 200µl of Milli Q water and incubated at 37℃ for more than 3hrs.

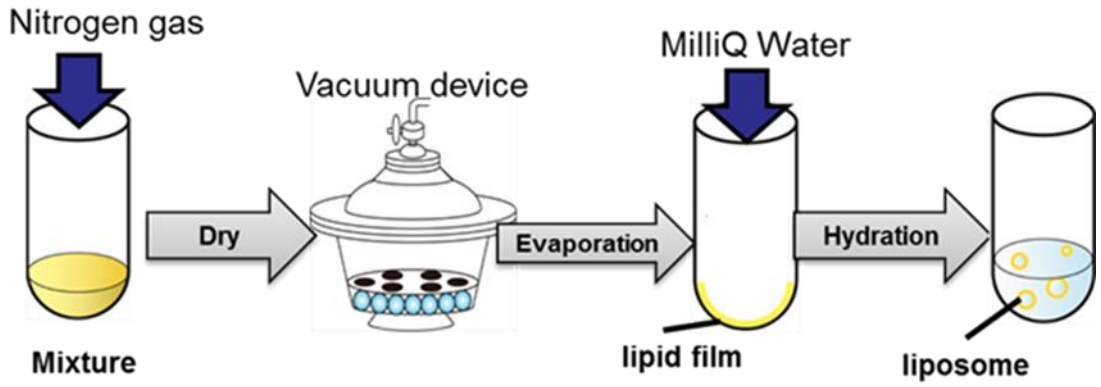

Fig. 2-3 Schematic of liposome preparation

2-2-3 Chamber preparation and liposome dynamics observation

Silicon rubber film (0.2 mm, AS ONE) and silicon rubber sheet (2.0 mm, AS ONE) were cut into 1.5 cm squares and 3 cm squares, respectively. Then, a 5 mm diameter hole was punched in the center of them. A 0.4μm pore filter (0,4 μm, Nucleopore, Whatman) was put between two pieces of silicon rubber film. This was then placed on a rubber sheet so that the holes overlap. 8μl of GUV solution was added to the hole from the silicon rubber film side and was covered with a slide glass (30 × 40 mm, MATSUNAMI) (Fig. 2-4). The chamber was placed with the slide glass down and the GUVs solution was observed using a confocal laser scanning microscopy (FV-1000, Olympus, Tokyo, Japan) (Fig. 2-5). After finding an appropriate GUV, we started to record the dynamics of the GUV. Ten seconds after the start of recording, 32 μl of surfactant which is adjusted to pH 6.2 was added to the hole from the rubber sheet side. The existence of a 0.4 μm pore filter help surfactants diffuse slowly and slows the movement of a GUV in the field of view. This record was finished when membrane dynamics reached equilibrium.

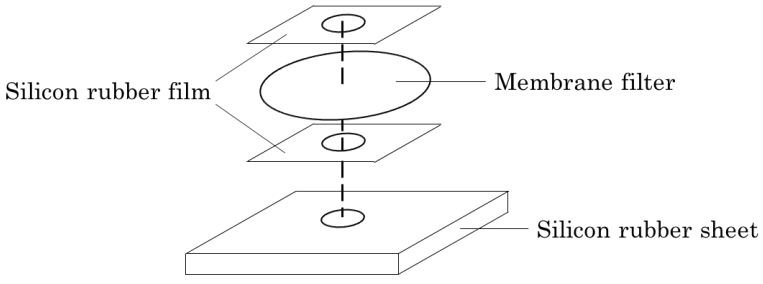

Fig. 2-4 Preparation of chamber for the observation

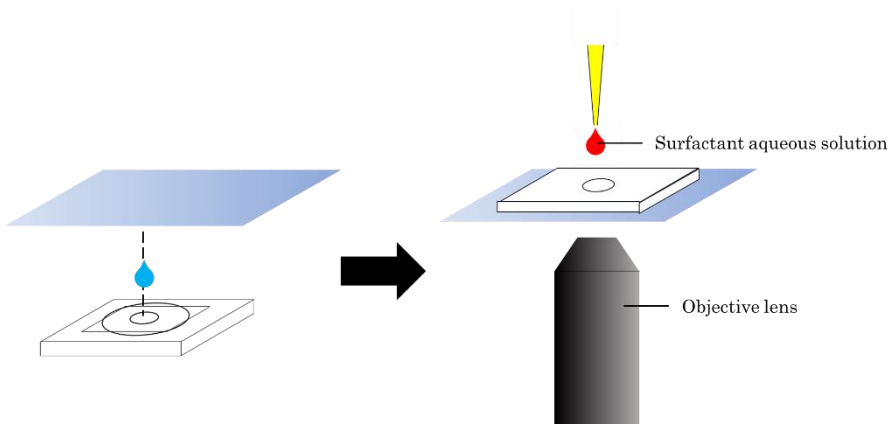

Fig. 2-5 Microscopy method

2-2-4 Liposome Dynamics Method for Evaluation of Stimulation

Membrane dynamics depending on the stimulus intensity are shown below (Fig. 2-6).

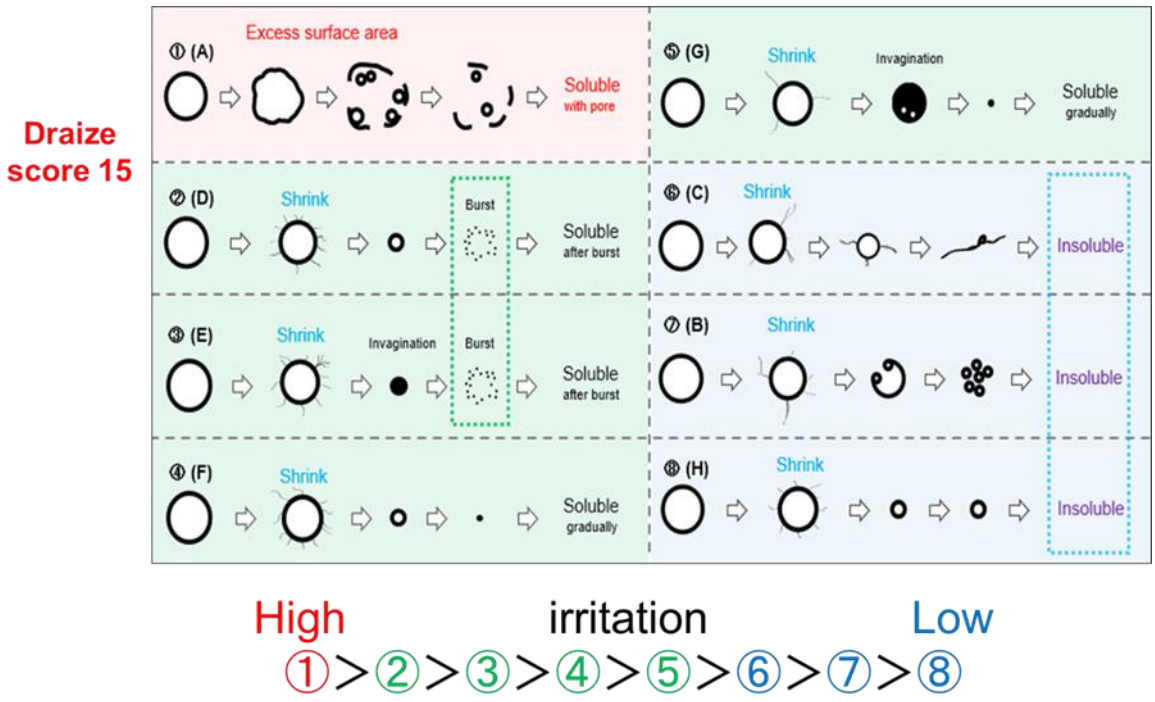

Fig. 2-6: Eight different membrane dynamics corresponding to strength of irritation

2-2-5 Stinging test

A non-woven gauze soaked with 1 mL of various surfactants was applied to the subject's posterior neck with surgical tape, and immediately thereafter, a hearing was conducted every 1 minute. Hearings were recorded up to 10 minutes after the gauze was applied.

2-2-6 LUV preparation for the measurement of the rate of Flip-Flop

Large unilamellar vesicles (LUVs) were prepared for measuring the rate of flip-flop ($V_{Flip\text{-}Flop}$) (Fig. 2-6). DOPC and tween 20 were dissolved in chloroform to 60mM and 30mM, respectively. NBD-DPPE was dissolved in chloroform to 0.6 mM. First, we prepared a lipid mixture composed of 40µl DOPC and 40µl NBD-DPPE in a durham tube. Tween 20 was added there in any proportion, and we mixed them. Secondly, the lipid mixtures were dried with N_2 gas to make lipid films and we keep them under vacuum for more than 3 hours to eliminate the rest organic solvent. Thirdly, lipid films were added with 400µl 10mM Tris/154mM NaCl buffer (pH 7.4) to the final concentration 6mM (DOPC) and 0.06mM (NBD-DPPE), respectively, then vortexed and sonicated at room temperature at which is higher than the main transition temperature of DOPC(-17℃) for 1 hrs to obtain multi-lamellar vesicles (MLVs). After sonication, the MLVs were extruded 13× successively through a series of three different-sized (1.0, 0.4, and 0.1 µm) nucleopore filters using a mini-extruder.

After extrusion, LUVs were exposed to 1M sodium dithionate in Tris aq and gently mixed by pipetting to quench the NBD on the outer leaflet of LUVs (Fig. 2-7). The dithionate quenches NBD by chemical modification, which is an irreversible reaction. Since dithionate can diffuse across the bilayer and quench NBD in the inner leaflet, dithionate in the quenched LUVs solutions was immediately removed with the desalting column superdex 200(Armstrong et al., 2003; John et al., 2002). Desalted LUVs have fluorescent NBD-DPPE on their inner leaflet and quenched NBD-DPPE in their outer leaflet. We called them “asymmetric LUVs (ALUVs)”.

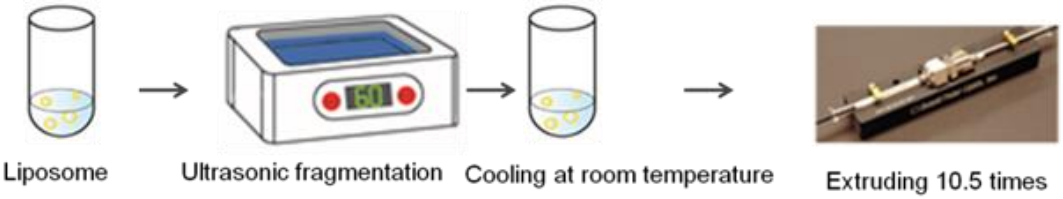

Fig. 2-6 Schematic of LUV preparation

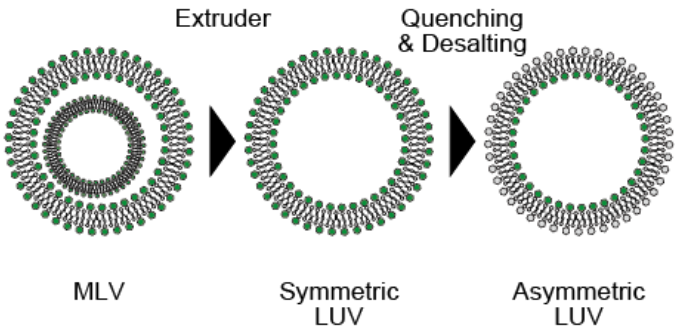

Fig. 2-7 Schematic of liposome preparation

2-2-7 Fluorescence measurements for Flip-Flop

We measured the ratio of fluorescence intensity before and after adding sodium dithionate at each time (Fig. 2-8 a). The detailed procedure is shown below. (i) Fluorescence intensity of ALUVs incubated indicated time (I_0) was measured for 200 sec. (ii) 5μl Sodium dithionate (1M; Tris aq) was added to the sample and mixed by pipetting for 40 sec. (iii) Fluorescence intensity of ALUVs containing no fluorescent NBD on their outer leaflet (I) was measured for 300sec. We calculated I/I_0 and plotted it at each time. Then the plots were fitted using the following equation (Fig. 2-8 b). The rate of NBD-DPPE flip-flop is given by

$$\frac{dn_i}{dt} = -k_o n_i + k_i n_o \quad (1)$$

where n_i and n_o are the numbers of NBD-DPPE molecules in the inner leaflet and outer leaflet, respectively, and k_i and k_o are rate constants of flip (movement from outer leaflet to inner leaflet) and flop(movement from inner leaflet to outer leaflet) respectively. ALUVs incubated 0 min have n_o= 0 and n_i=N of fluorescence NBD-DPPE. N (=n_i+n_o) does not change during flip-flop. Under these conditions, we can solve the differential equation (Eq. (1)) analytically and obtain the following expression.

$$n_i = \frac{1}{2}N(1 + e^{-(k_i+k_o)t}) \quad (2)$$

where k=k_i+k_o is the total flip-flop rate constant.

Since fluorescence intensity is proportional to the number of molecules, it can be rewritten as follows

$$I = \frac{1}{2} I_0 \left(1 + e^{-(k_i + k_o)t}\right) \quad (3)$$

To correct the delay caused by the operation of quenching and desalination, a time *T* was introduced.

$$I = \frac{1}{2} I_0 (1 + e^{-(k_i + k_o)(t+T)}) \quad (4)$$

The half-time of this process ($t_{1/2}$) was given by

$$t_{1/2} = \frac{In2}{k_i + k_o} \quad (5)$$

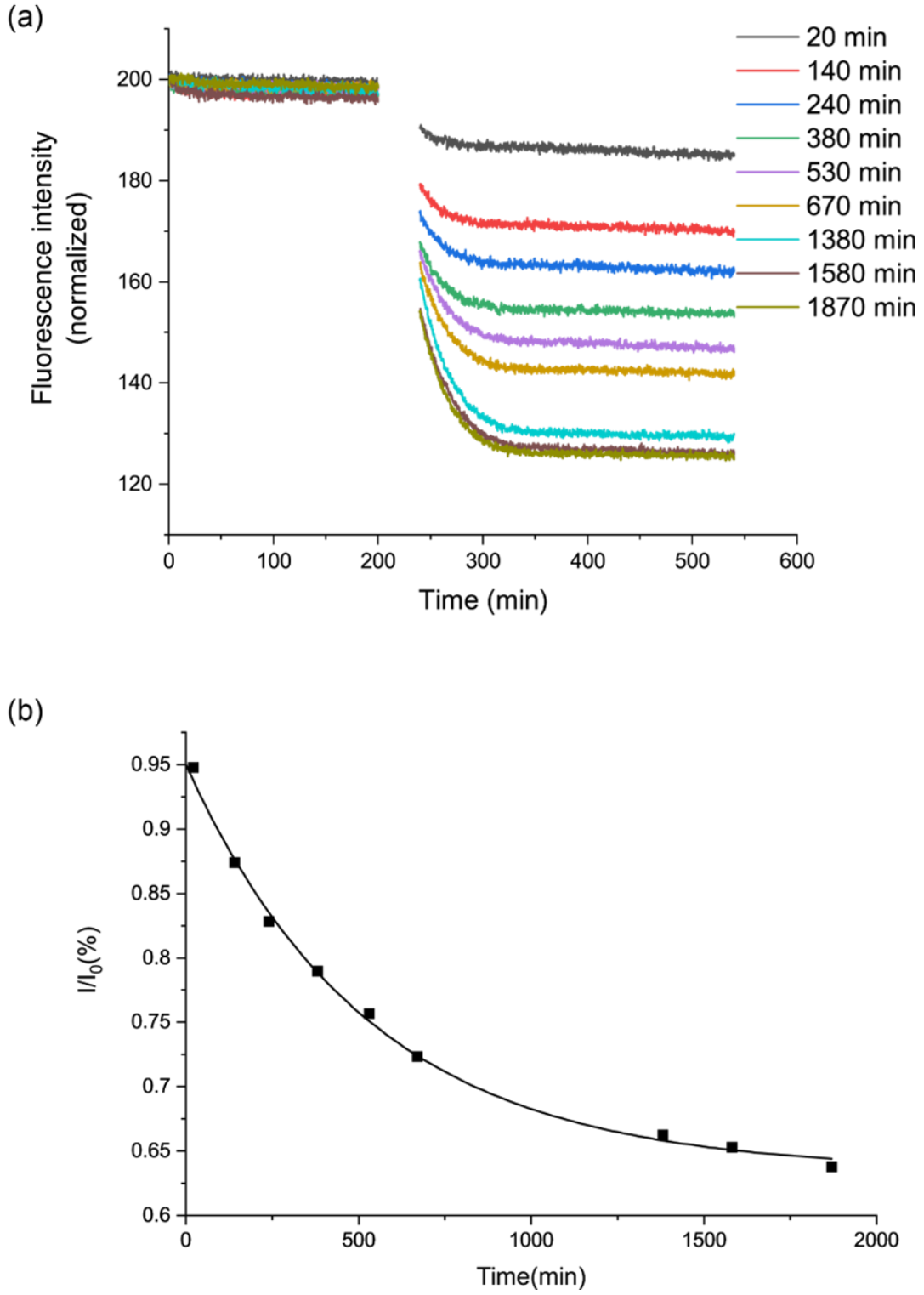

Fig. 2-8 NBD-DPPE in DOPC LUV containing 5% tween20 (a) An example of fluorescence measurement of time drives course after incubating ALUVs for the indicated time (b)Best fit to data obtained at each time

2-3 Results

2-3-1 Membrane dynamics induced by surfactants

2-3-1-1 Amino acids surfactants

(A)

We conducted irritancy tests on sodium lauroyl glutamate, which is a main component of sodium cocoyl glutamate (Fig. 2-9). By adding 14mM sodium lauroyl glutamate, the GUV shrank then, an insoluble structure was formed (Dynamics ⑧). By adding 28mM sodium lauroyl glutamate, GUVs showed swelling and fluctuation. Subsequently, a small vesicle was formed inside the GUV. Although this is an unclassified dynamics, we considered it to be more stimulating than the shrank dynamics because it is similar to dynamics ①, showing an increase in excess membrane surface area.

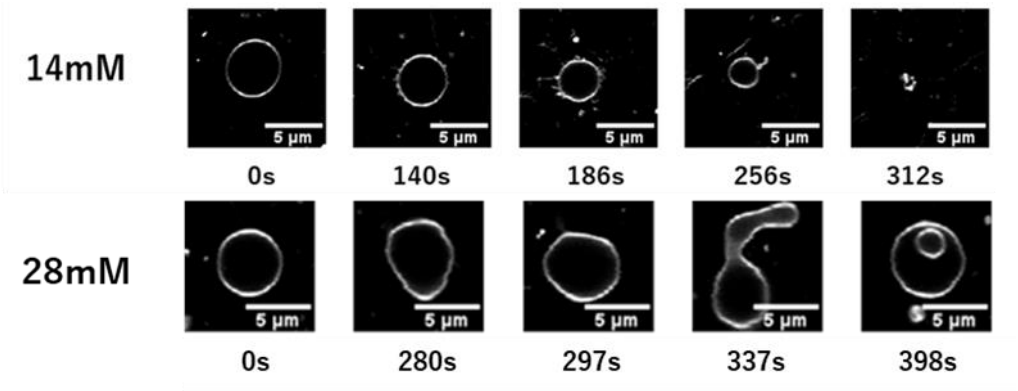

Fig. 2-9 Microscopic observation images with sodium lauroyl glutamate (pH 6.2)

2-3-1-2 Amino acids surfactants＋Amphoteric surfactant

Next, we investigated the effect of amphoteric surfactants on the irritation of amino acid surfactants.

2-3-1-2 (A) Sodium Lauroyl Glutamate+Cocamidopropyl Betaine

Cocamidopropyl betaine was added to sodium lauroyl glutamate in any ratio and adjusted to pH 6.2. At sodium lauroyl glutamate/cocamidopropyl betaine mixtures(= 3:1 and 2:1), the GUVs increase in excess surface area, followed by equilibilium (Fig. 2-10). Although these dynamics are unclassified dynamics, we considered them to be more stimulating than the shrank dynamics because it is similar to dynamics ①, showing an increase in excess membrane surface area. The ratio of cocamidopropyl betain increasing (to sodium lauroylglutamate/cocamidopropyl betaine (= 1:1)), GUVs shrank and dynamics reached equilibrium (dynamics ⑧).

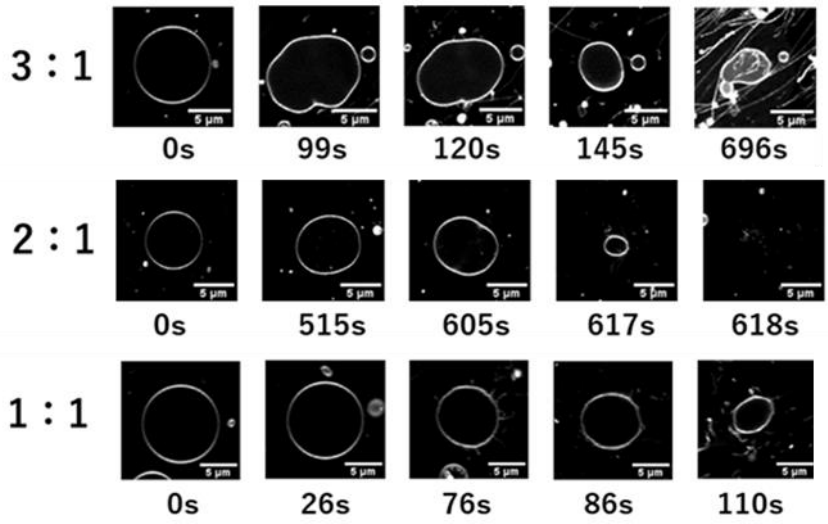

Fig. 2-10 Microscopic observation images with sodium lauroyl glutamate and cocamidopropyl betaine (pH 6.2)

2-3-1-2 (B) Sodium Lauroyl Glutamate + Lauramidopropyl Betaine

Sodium cocoyl glutamate was adjusted to pH 6.2 by adding lauramidopropyl betaine in any ratio. By adding sodium cocoylglutamate/lauramidopropyl betaine = 3:1, the excess surface area increased and then dynamics ceased (Fig. 2-11). By adding sodium cocoylglutamate/lauramidopropyl betaine = 2:1, GUVs shrank and then dynamics ceased. By adding sodium cocoylglutamate/lauramidopropyl betaine=1:1, the GUVs expands, deformation and finally shrank and ruptureed. Although these dynamics are unclassified dynamics, we considered them to be more stimulating than the shrank dynamics because it is similar to dynamics ①, showing an increase in excess membrane surface area.

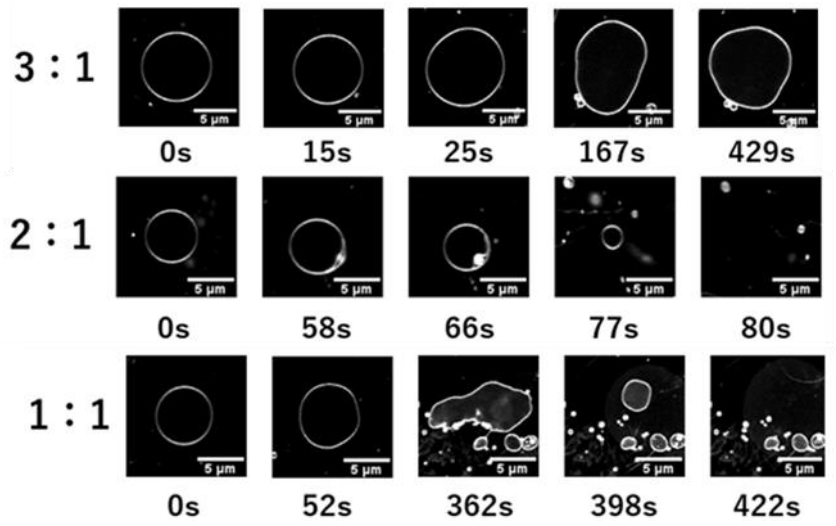

Fig. 2-11 Microscopic observation images with sodium lauroyl glutamate and lauramidopropyl betaine (pH 6.2)

2-3-2 Stinging test

Stinging tests were performed using surfactants with the same composition as in the liposome test. 0.5% sodium lauroyl glutamate had a maximum irritation score of 14.0. Next, 0.5% sodium lauroyl glutamate and cocamidopropyl betaine were mixed at the ratios shown in table. 1 and examined for irritation. As the amount of cocamidopropyl betaine was increased, the irritancy decreased. The maximum irritation score was 9.0 when the ratio of sodium lauroyl glutamate to cocamidopropyl betaine was 1:1, and the minimum irritation score was 9.0 when the ratio of sodium lauroyl glutamate to cocamidopropyl betaine was 1:1.

Next, the irritancy was examined by mixing 0.5% sodium lauroyl glutamate and lauramidopropyl betaine in the ratios shown. As lauramidopropyl betaine was increased, the irritancy became stronger. The maximum irritation score was 9.0 when the ratio of sodium lauroyl glutamate to lauramidopropyl betaine was 3:1, and the lowest when the ratio of sodium lauroyl glutamate to lauramidopropyl betaine was 3:1.

Mixed systems of amino acid surfactants and amphoteric surfactant					
Specimen		Anion: amophoteric	Maximum stimulus score	Maximum non-itch irritation score	Maximum itch score
Anion	amphoteric				
0.50%Sodium Lauroyl Glutamate		1 : 0	14.0	11.0	9.0
0.50%Sodium Lauroyl Glutamate	0.17%Cocamidopropyl Betaine	3 : 1	11.0	10.0	3.0
0.50%Sodium Lauroyl Glutamate	0.25%Cocamidopropyl Betaine	2 : 1	10.0	6.0	4.0
0.50%Sodium Lauroyl Glutamate	0.50%Cocamidopropyl Betaine	1 : 1	9.0	8.0	1.0
0.50%Sodium Lauroyl Glutamate	0.17%lauramidopropyl Beitaine	3 : 1	9.0	7.0	2.0
0.50%Sodium Lauroyl Glutamate	0.25%lauramidopropyl Beitaine	2 : 1	14.0	11.0	3.0

Table. 1　Results of stinging test

2-3-3 The rate of Flip-Flop

Membrane deformation is caused by a change in the number of molecules in the outer and inner leaflets of the bilayer. We hypothesized that the addition of surfactant to the LUV solution would increase the $V_{Flip\text{-}Flop}$. The $V_{Flip\text{-}Flop}$ was measured using ALUVs. ALUVs were incubated for any time, and we obtained the ratio of fluorescence intensity of NBD-DPPE before and after quenching by dithionate (I/I_0). As Flip-Flop progresses, the apparent fluorescent NBD-DPPE moves to the outer leaflet of the bilayer, and the decrease in I/I_0 becomes greater. When Flip-Flop reaches equilibrium, I/I_0 becomes stable. As a control, the $V_{Flip\text{-}Flop}$ of NBD-DPPE in DOPC LUVs was measured (Fig. 2-12). The rate of $V_{Flip\text{-}Flop}$ was 0.068 ± 0.006 (h^{-1}) (Table 2).

Next, to reveal the effect of tween 20 on the transbilayer movement of NBD-DPPE in DOPC LUV, the $V_{Flip\text{-}Flop}$ was measured using DOPC LUVs containing tween 20 (Fig. 2 and Table2). Tween20 2.5% and 5% slightly increased the $V_{Flip\text{-}Flop,}$ 0.11 ± 0.011 (h^{-1}) and 0.14 ± 0.014 (h^{-1}), respectively. Adding 20% tween20 significantly increased the $V_{Flip\text{-}Flop}$ (3.29 ± 1.2 (h^{-1})). The $V_{Flip\text{-}Flop}$ was increased with higher tween20 concentrations.

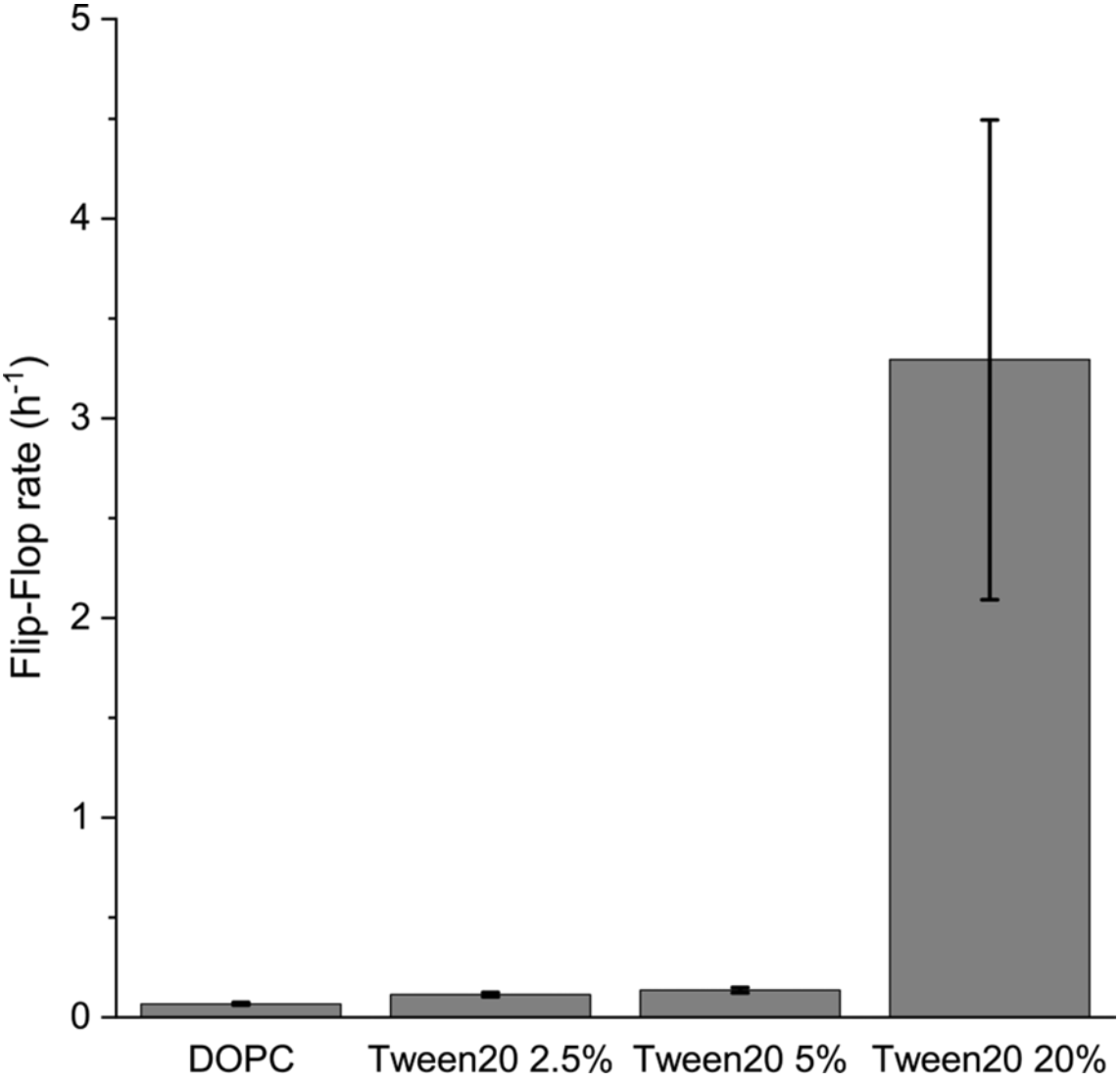

Fig. 2-12 Flip-Flop rate of NBD-DPPE in LUVs containing tween20. The measurements were conducted at room temperature.

	$t_{1/2}$ (h)	$V_{flip\text{-}flop}(h^{-1})$
DOPC	10.9±0.99	0.068±0.006
Tween20 2.5%	6.15±0.56	0.11±0.011
Tween20 5%	5.22±0.54	0.14±0.014
Tween20 20%	0.29±0.11	3.29±1.20

Table 2 Parameters obtained from the fluorescence measurement for the rate of transbilayer movement of NBD-DPPE in LUVs containing tween20

2-4 Discussion

2-4-1 Surfactant-induced membrane dynamics

Surfactant-induced dynamics, with high-irritating surfactants, increasing the excess surface area and low-irritating and non-irritating surfactants shrinking the liposomes.

To discuss membrane dynamics, we consider the following three rates (Fig. 2-13)

V_{in} : The rate at which the surfactants are incorporated into the liposome

$V_{Flip\text{-}Flop}$: Flip Flop rates of surfactant and membrane lipid

V_{out} : Rate at which lipid and surfactant form micelles and solubilize

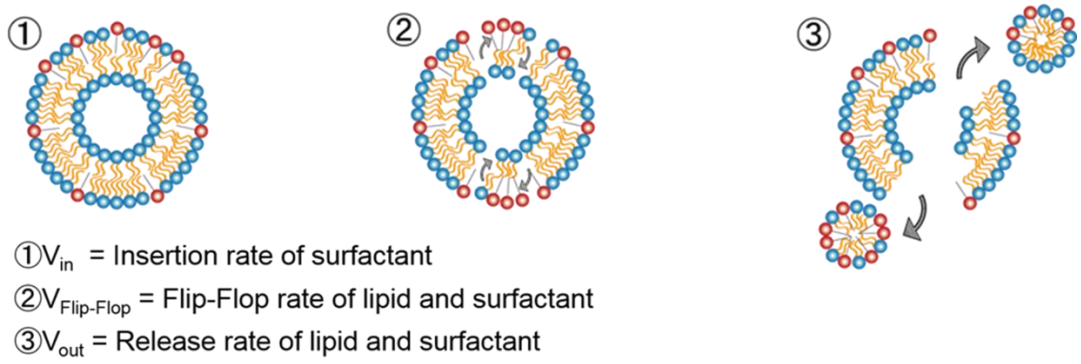

Fig. 2-13 Definition of V_{in}, V_{out} and $V_{Flip\text{-}Flop}$

<u>○Sodium Lauroyl Glutaminate</u>

[14mM] Membrane shrank was observed. This indicated that V_{out} is fast rather than V_{in} and $V_{Flip\text{-}Flop}$. $V_{out}>V_{Flip\text{-}Flop}>V_{in}$

[28mM] An increase in excess film surface area was observed. This indicates that the surfactant inserted into the outer membrane immediately migrated to the inner membrane. Thus, Vin and VFlip-Flop are likely to be fast. Vin≈VFlip-Flop≥Vout.

○Sodium Lauroyl Glutamate+Cocamidopropyl Betaine

[3: 1 and 2: 1]

The relationship between the velocities of V_{in} V_{out} $V_{Flip\text{-}Flop}$ changes with time.

Initially, Vin and $V_{Flip\text{-}Flop}$ may be faster than V_{out} because the membrane is expanding. Subsequently, GUV's shrink was observed. This indicates that V_{out} became faster than V_{in}.

①$V_{in} \fallingdotseq V_{Flip\text{-}Flop} > V_{out}$

②$V_{out} > V_{in} > V_{Flip\text{-}Flop}$

[1: 1]

V_{out} is the fastest because the membrane shrank, and V_{in} and $V_{Flip\text{-}Flop}$ are slow.

$V_{out} > V_{in} > V_{Flip\text{-}Flop}$

○Sodium Lauroyl Glutamate+Lauramidopropyl Betaine

[3: 1]

The membrane is fluctuating, so V_{in} is the fastest, and V_{out} and $V_{Flip\text{-}Flop}$ are slow.

$V_{in} >> V_{Flip\text{-}Flop} \fallingdotseq V_{out}$

[2: 1]

V_{out} is fastest and V_{in} and $V_{Flip\text{-}Flop}$ are slowest because the membrane is shrinking and disappearing.

$V_{out} > V_{in} > V_{Flip\text{-}Flop}$

[1: 1]

Initially, the membrane is fluctuating, so V_{in} is the fastest. Subsequently, V_{out} becomes fastest and V_{in} and $V_{Flip\text{-}Flop}$ become slow because the membrane is shrinking and disappearing.

① $V_{in} >> V_{Flip\text{-}Flop} > V_{out}$

② $V_{out} > V_{in} > V_{Flip\text{-}Flop}$

2-4-2 The rate of Flip-Flop

We showed that $V_{Flip\text{-}Flop}$ was increased in the presence of tween20. Flip-Flop was faster as the concentration of tween 20 was increased. Previous studies have shown that a decrease in membrane order increases the $V_{Flip\text{-}Flop}$. Therefore, it was suggested that tween20 inserts into the membrane and decreases the intermolecular interactions of phospholipids.

In this study, we have shown that even surfactants that do not cause membrane rupture are irritating in stinging tests. Lipid bilayers are not permeable to ions. Since these surfactants cause an increase in the excess membrane surface area of GUVs, it is possible that Flip-Flop or the distribution of surfactant molecules into the membrane may cause Ca^{2+} influx. The relationship between lipid membrane order and Ca^{2+} influx, which triggers an inflammatory response, needs further investigation.

Chapter 3
ER stress model membrane

3-1 Introduction

Cells maintain homeostasis and perform their roles properly. The endoplasmic reticulum (ER) plays an important function in protein and lipid homeostasis. When the homeostasis is disrupted, ER stress occurs, causing various diseases. Highly conserved, ER stress sensor proteins are present in the ER membrane. They are activated by increased misfolding in the ER lumen, and saturation of ER membrane, which initiates unfolded protein responses (UPR)(Radanović and Ernst, 2021; Szegezdi et al., 2006; Tabas and Ron, 2011). The UPR copes with misfolded protein by increasing protein folding ability, decreasing newly protein synthesis, and promoting ER associated degradation. If these processes cannot alleviate ER stress, cell death was induced.

Amyloid-β (Aβ) is a misfolding protein and accumulation of Aβ causes ER stress, leading to Alzheimer's disease (AD)(Nakagawa et al., 2000; Umeda et al., 2011). Aβ has 40-42 amino acid residues, including amino acids in the transmembrane region of amyloid precursor protein (APP). Since the transmembrane region is highly hydrophobic, Aβ prone to polymerize spontaneously in cells. Aggregation of Aβ consisting of 42 amino acids (Aβ42) is faster than that of Aβ40 and is reported to be highly toxic. The toxicity of Aβ also varies depending on the degree of polymerization, with intermediates to the fibrillar structure being highly toxic.

Previous studies have shown that Aβ oligomer and protofibril, highly toxic Aβ species, have a greater impact on membrane dynamics than monomer and fibril, less toxic species(Korshavn et al., 2017; Sciacca et al., 2012). Furthermore, our previous study found that highly toxic oligomer and protofibril of Aβ tend to accumulate on solid-ordered (S_o) phase, rich in saturated lipid, rather than liquid-disordered (L_d) phase, rich

in unsaturated lipids(Hamada et al., 2010; Morita et al., 2012; Phan et al., 2014). Surprisingly, oligomer and protofibril of Aβ tend to accumulate on L_d phase rather than liquid-ordered (L_o) phase, rich in saturated lipids and cholesterol (Chol).

Unlike cell membrane, ER membranes are known to have low Chol content and form the S_o phase(Jacquemyn et al., 2017; Tian et al., 2022; van Meer et al., 2008). Therefore, the formation of S_o phase at the ER membrane may cause accumulation of denatured proteins, leading to ER stress.

Plasma Vitamin E (VE) concentration is thought to be associated with a variety of diseases such as Alzheimer's disease (AD) which is induced by ER stress(Browne et al., 2019; Mangialasche et al., 2012, 2010). Many epidemiological studies have reported that blood VE levels are decreased in AD patients. On the other hand, some reports show no difference in blood VE levels between AD patients and healthy subjects. A possible reason for the discrepancy in results is that the onset of AD is multifactorial.

VE, discovered as a factor that inhibits infertility in 1922 by Evens and Bishop, is a fat-soluble molecule(Evans and Bishop, 1922). Vitamin E has a chromanon ring with hydrocarbon groups on the side chain. There are four methylation states of chromanon rings: α -, β-, γ-, and δ-. Side chains include phytyl or farnesyl groups. Those with phytyl groups are called tocopherols and those with farnesyl groups are called tocotrienols. The phytyland farnesyl groups have different degrees of double bond saturation. The phytyl group is saturated, while the farnesyl group has three double bonds. Previous study showed that this difference makes tocotrienols more hydrophilic than tocopherols if the methylation state of chromanon rings is the same(Kamal-Eldin et al., 2000).

Recently, it has been reported that α-tocopherol (Toc), but not α-tocotrienol (Toc3),

reduces ER stress caused by 24S-hydroxycholesterol (24S-OHC), which is related to AD(Kimura et al., 2018; Nakazawa et al., 2017; Urano et al., 2019). Toc and Toc3 are present in biological membranes and have different effects on ER membrane properties.

Unlike cell membrane, ER membranes are known to have low Chol content and form the S_o phase, rich in saturated lipids(Jacquemyn et al., 2017; Tian et al., 2022; van Meer et al., 2008). Biomimetic membranes can form a variety of phase states such as S_o, L_d, and L_o phases(Veatch and Keller, 2005, 2003). Therefore, we prepared a Chol-free biomimetic membrane that forms S_o phase as a model for the ER stress membranes and Chol containing biomimetic membrane that forms L_o phase as a model for lipid raft. In this study, we clarify the effect of Toc and Toc3 on the Aβ adsorption onto ER stress mimicking membranes and raft mimicking membrane.

3-2 Materials and Methods

3-2-1 Material

Unsaturated lipid, 1,2-dioleoyl-*sn*-glycero-3-phosphocholine (DOPC)、saturated lipid, 1,2-dipalmitoyl-*sn*-glycero-3-phosphocholine (DPPC) and Cholesterol (ovine) (Chol) were purchased from Avanti Polar Lipid (Alabaster, USA). To label unsaturated lipid rich, liquid disordered (L_d) phase, lissamine™ rhodamine B 1,2-dihexadecanoyl-*sn*-glycero-3-phosphoethanolamine, triethylammonium salt (Rhodamine-DHPE) (λex = 560 nm, λem = 580 nm) was used. Rhodamine-DHPE was purchased from Thermo Fisher (Waltham, USA). To measure lipid membrane order, 1,6-diphenyl-1,3,5-hexatriene (DPH) was used. DPH was purchased from Sigma Aldrich (Missouri, USA). β-Amyloid (1-42, human) (Aβ) was purchased from Peptide Institute Inc. (Japan). The amino acid sequence of Aβ was as follows: NH_3-Asp-Ala-Glu-Phe-Arg-His-Asp-Ser-Gly-Tyr-Glu-Val-His-His-Gln-Lys-Leu-Val-Phe-Phe-Ala-Glu-Asp-Val-Gly-Ser-Asn-Lys-Gly-Ala-Ile-Ile-Gly-Leu-Met-Val-Gly-Gly-Val-Val-Ile-Ala-OH, Aβ (1-42, human) HiLyte Fluor 488 Conjugate (Aβ488) (λex = 503 nm, λex = 528 nm) was purchased from Anaspec, Inc. (USA). Hilyte™ Fluor488 was conjugated to N-terminus of Aβ (1-42). Toc and Toc3 were kindly provided by Dr. Noriko Noguchi and Dr. Yasuomi Urano, in Doshisha university.

DPPC

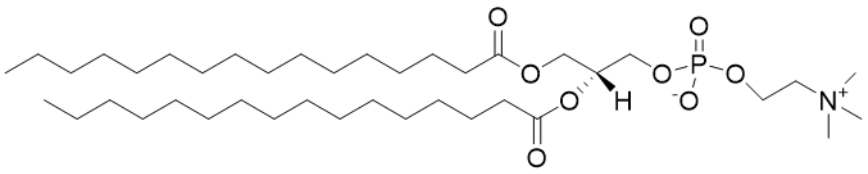

DOPC

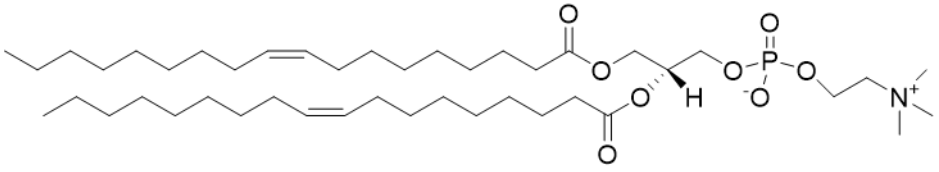

Cholesterol (Chol)

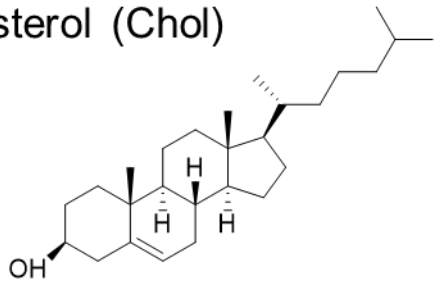

α-Tocopherol (Toc)

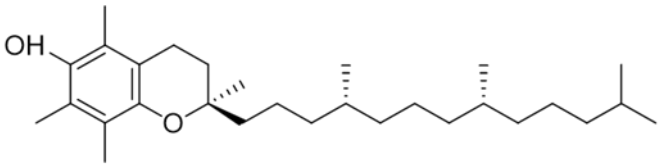

α-Tocotrienol (Toc3)

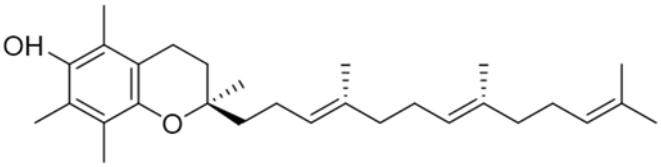

Rhodamine-DHPE

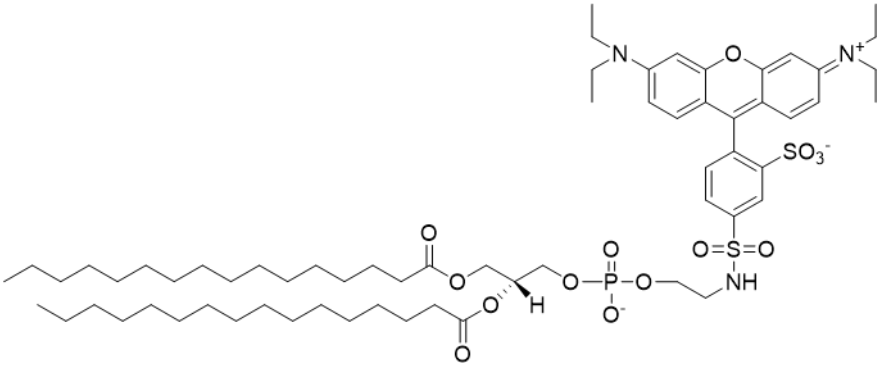

DPH

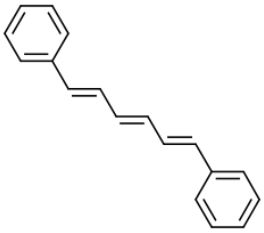

Fig. 3-1 Chemical structures of lipids, VEs, and fluorescence probes

3-2-2 GUV preparation for microscopy observation

In this chapter, giant unilamellar vesicles (GUVs) were used for microscopy observation and prepared by the natural swelling method (Fig. 3-2). Lipids (DOPC, DPPC, Chol) and VE (Toc, Toc3) were dissolved in chloroform/methanol (2: 1 v/v) to 2mM. Rhodamine-DHPE, L_d phase marker, was dissolved in chloroform to 0.1mM. Firstly, we prepared lipid mixtures composed of DPPC, DOPC, Chol, Toc, Toc3, and 2μl Rhodamine-DHPE (0.1mM) in a durham tube. In the ternary system, the ratio of DOPC/DPPC/Chol (1:1:0) was fixed and Toc or Toc3 was added in any ratio, making the total volume 20 μl. In the quaternary system, the ratio of DOPC/DPPC/Chol (2:2:1) was fixed and Toc or Toc3 was added in any ratio, making the total volume 20 μl. Secondly, the lipid mixtures were dried with N_2 gas to make lipid films and we keep them under vacuum for more than 3 hours. The vacuum environment was prepared with a vacuum pump and a desiccator. Finally, lipid films were added with 200 of Milli Q water and leave them in the incubator in which the temperature was kept at 37℃ for more than 3 hours to spontaneously induce GUVs.

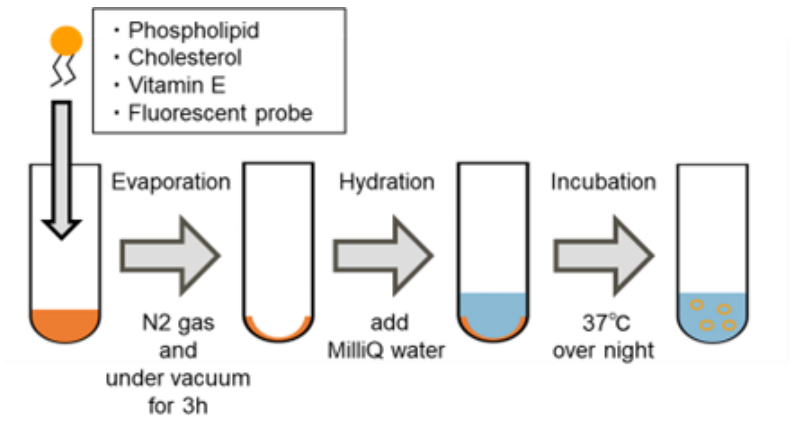

Fig. 3-2 Schematic of natural swelling method

3-2-3 GUV observation at room temperature

To observe GUV, we prepared a chamber (Fig. 3-3). A silicone film with holes was attached to a slide glass. Then GUV solution was added to the hole of silicon film and the hole was covered with cover glass. GUV solution was observed at room temperature using a fluorescent microscope (IX 71, Olympus, Tokyo, Japan). All observation was conducted within 90 sec to avoid photo-induced lipid oxidization. We counted GUVs more than 100 in each condition.

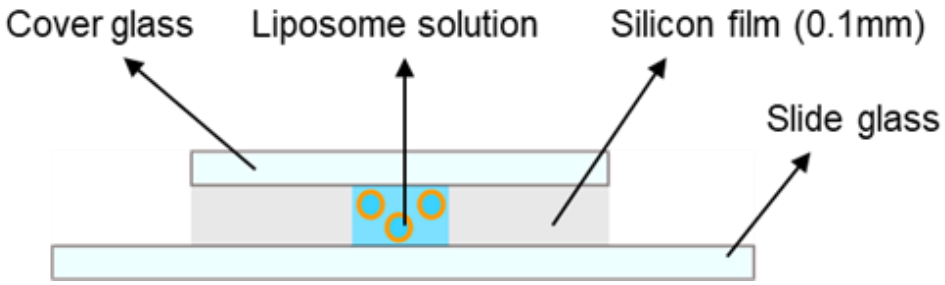

Fig. 3-3 Schematic of observation sample

3-2-4 Temperature control for microscopic observation

To observe GUVs, at any temperature, thermo-plate (MATS-555ORA-BT, TOKAI HIT) was used (Fig. 3-4). The observation chamber was placed on the thermo-plate and GUV solution was adjusted to the desired temperature. We used thermocouple thermometer (AS ONE) and measured the temperature of a cover glass. The temperature on the cover glass was regarded as GUV solution temperature in this measurement. After the GUV temperature reached the desired temperature, we maintained the temperature (±0.5℃) for 5 min until the sample reached the equilibrium state. Following the temperature control, observation was started with a fluorescence microscopy (IX 71, Olympus) and counted more than 60 GUVs for 90 sec.

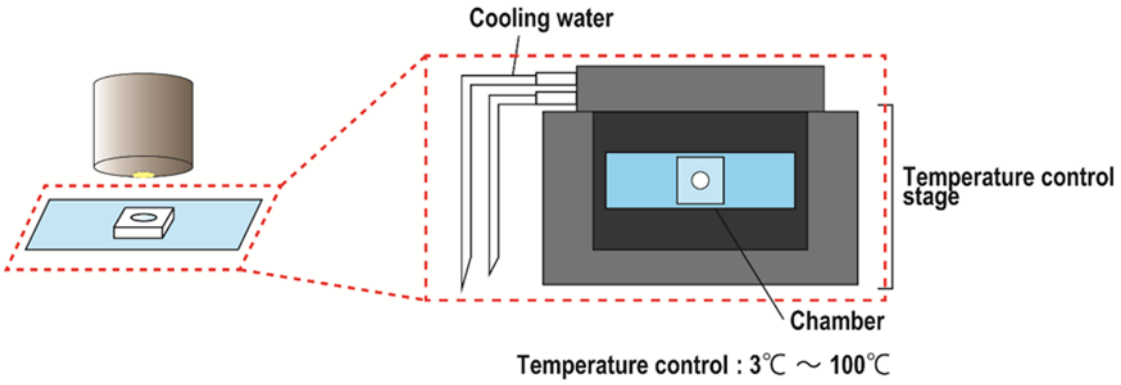

Fig. 3-4 Schematic of temperature control

3-2-5 Miscibility temperature measurement

To understand the thermal stability of phase separated structure, we calculated miscibility temperature (T_{mix}). T_{mix} is defined as the temperature at which the fraction of phase separated GUVs is 50%. To obtain T_{mix}, we measured the fraction of phase separated GUVs at each temperature and the fractions were plotted. The plotted data were fitted with a sigmoid Boltzmann function, and T_{mix} was calculated. The sigmoid Boltzmann function is shown below.

$$P = \frac{1}{1 + \exp[(T - T_{\mathrm{mix}})/dt]}$$

where P is the fraction of phase separated GUVs, T is the temperature, and dt is the slope of the sigmoidal curve

3-2-6 MLV preparation for differential scanning calorimetry

Multi lamellar vesicles (MLVs) were used for differential scanning calorimetry (DSC) (Fig. 3-5). Lipids (DPPC, Chol), Toc, and Toc3 were dissolved in chloroform to 300 mM. First, we prepared lipid mixture composed of DPPC, DOPC, Chol, Toc, and Toc3 in durham tube. In the binary system, DPPC and Toc or Toc3 were mixed in any ratio, making the total volume 30 µl. In the ternary system, the ratio of DPPC/Chol (9:1) was fixed and Toc or Toc3 was added in any ratio, making the total volume 30 µl. Secondly, the lipid mixtures were dried with N_2 gas to make lipid films and we keep them under a vacuum for more than 3 hours. The vacuum environment was prepared with a vacuum pump and a desiccator. Finally, lipid films were added by MilliQ water to the final concentration 150 mM, vortexed and sonicate at T>60℃ which is higher than the main transition temperature of DPPC (42℃) for 1 hr.

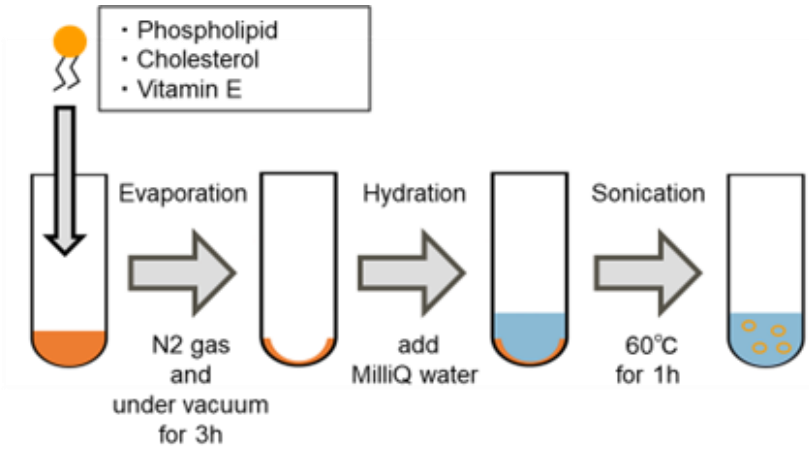

Fig. 3-5 Schematic of MLV preparation for DSC measurement

3-2-7 Differential scanning calorimetry

To investigate the thermal stability of lipid membranes containing VE, we used DSC to measure the change in phase transition temperature (T_m). Lipids undergo a phase transition from the gel phase to the liquid crystal phase when the temperature is increased from the low temperature side. The phase transition is accompanied by an endothermic reaction, which can be detected by DSC.

13 (±0.2mg) mg of MLV solution was placed in an aluminum pan (ME-27331). As the reference sample pan, an aluminum sample pan was filled with the same amount of Milli-Q water as contained in the sample. The sample and reference sample pans were set in a DSC822 (Mettler Toledo) and subjected to three heating and cooling cycles. Heating and cooling were conducted under the following conditions: 20~60°C (heating/cooling temperature 5°C/min) andN_2gas inflow 75 ml/min. Heating and cooling were performed as follows: (1) 10°C was maintained for 5 minutes, (2) then heated to 60°C at 5°C/min, (3) maintained at 60°C for 3 minutes, and (4) cooled at 5°C/min. Three cycles were performed with (1) to (4) as one cycle. As the representative result, the data from the third cycle of heating was used. The same measurements were performed at least three times to ensure data reproducibility. Thermographs were created with STARe software (Metter Toledo). Origin 2018 was used to analyze the asymmetric thermographs obtained (Fig. 3-6).

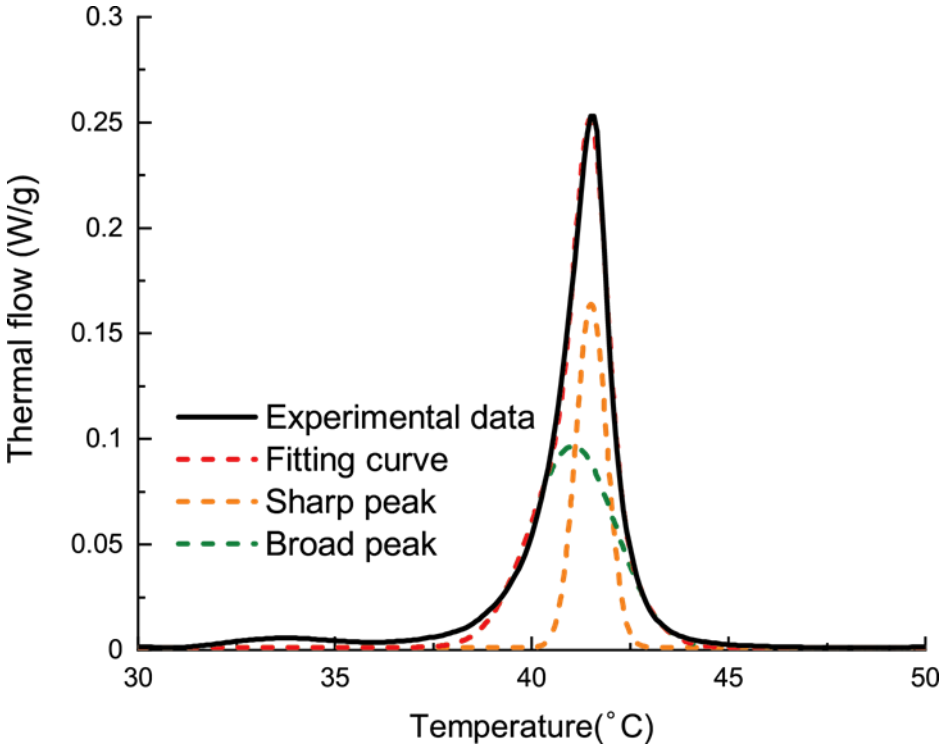

Fig. 3-6 An example of peak deconvolution for DPPC/Toc=97.5: 2.5. Black line represents the experimental data. The experimental data was deconvoluted into two symmetric peaks which were indicated by orange and green dashed lines. The sum of these two lines which was indicated by red dashed line was the fitting curve.

3-2-8 Line tension of L_o phase boundary

To calculate line tension, flicker spectroscopy was used (Esposito et al., 2007). In this method, we record the fluctuation of L_o domain boundary with 30 frames/sec for more than 3 sec, thus more than 90 frames. We did not measure the line tension of L_o domain which occur the coalescence with other domains and/or do not have clearly visible domain boundary during the recording. By using image J software, we obtained the binarized images. From the binarized images, we obtained the radial fluctuation r as a function of the polar angle ψ and used Fourier series expansion to represent the radial fluctuation.

$$r(\psi) = r_{av}[1 + a_0 + \sum_{k=1}^{\infty} a_k \, cos(k\psi) + \sum_{k=1}^{\infty} b_k sin(k\psi)]$$

where r_{av} is the average domain radius, ψ is the polar angle, k is the mode number, a_k and b_k are Fourier coefficients. The excess energy ΔF generated by the fluctuations can be expressed as,

$$\Delta F = \frac{\pi r_{av}}{2} \gamma \sum_{k=2}^{\infty} (k^2 - 1)(a_k^2 + b_k^2)$$

where γ is the line tension. According to the generalized equipartition theorem, free

energy for each independent mode is k_{bT} (kb is the Boltzmann constant). Thus, the following expression is obtained as,

$$\left(a_k^2\rangle + \langle b_k^2\rangle\right) r_{av} = \frac{2k_B T}{\pi\gamma}\left(\frac{1}{k^2-1}\right)$$

where $\langle a_k^2\rangle$ and $\langle b_k^2\rangle$ are the averaged Fourier coefficients of all images. According to Equation, the value of line tension can be derived by the liner regression equation between k and the Fourier coefficients $\langle a_k^2\rangle$ and $\langle b_k^2\rangle$。

3-2-9 MLV preparation for DPH anisotropy measurement

Multi lamellar vesicles (MLVs) were used for DPH measurement (Fig. 3-7). Lipids (DOPC) and VEs (Toc and Toc3) were dissolved in chloroform to 20 mM. DPH was dissolved in chloroform to 0.2 mM. First, we prepared a lipid mixture composed of DOPC, Chol, Toc, Toc3, and 30ml DPH in durham tube. DOPC, Chol, and VEs (Toc or Toc3) were mixed in any ratio, making the total volume 65 µl. Secondly, the lipid mixtures were dried with N_2 gas to make lipid films and we keep them under vacuum for more than 3 hours. The vacuum environment was prepared with a vacuum pump and a desiccator. Thirdly, Lipid films were added by 250µl MilliQ water to the final concentration 5.2 mM (lipids) and 0.0012 mM (DPH), respectively, vortexed and sonicated for 1 hr. After sonication, the MLVs were extruded 13× successively through 0.4 µm Nucleopore filters.

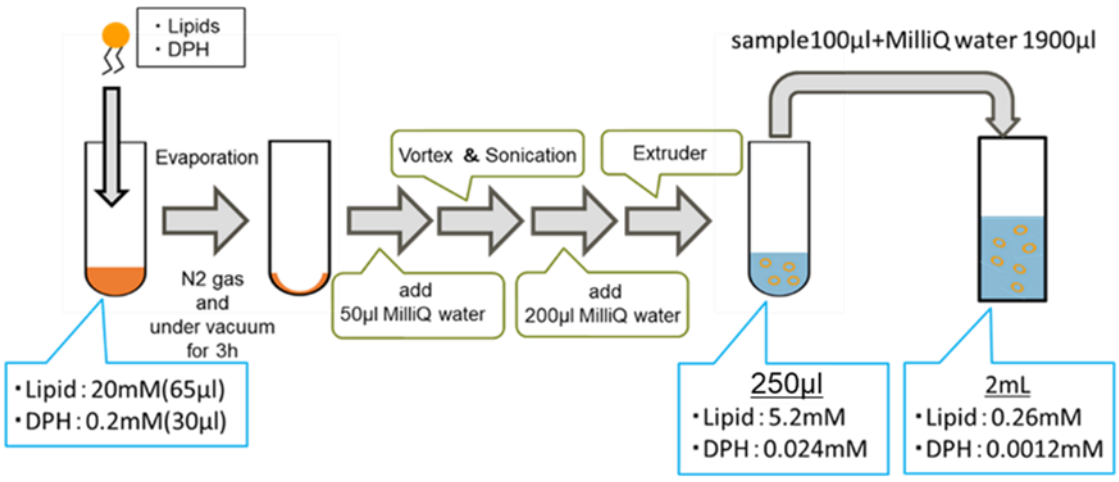

Fig. 3-7 Schematic of MLV preparation for DPH anisotropy measurement

3-2-10 DPH anisotropy

To compare the effect of Toc and Toc3 on L_d phase order, we measured the fluorescence anisotropy of DPH in lipid bilayers composed of DOPC and VE. DPH is inserted into the membrane and changes the velocity of molecular rotation depending on membrane order. In highly ordered membranes, DPH moves less, and in low-ordered membranes, the molecular motion of DPH is greater. Therefore, the fluorescence anisotropy changes depending on the membrane order. Highly ordered membranes have high fluorescence anisotropy, while low order membranes have low fluorescence anisotropy.

DPH measurement was performed using an FP-6500 spectrofluorometer (JASCO Co. Tokyo, Japan) at room temperature. Polarizers (JASCO Co. Tokyo, Japan) were attached to the excitation and emission sides.

Firstly, the vertical excitation light was selected, and the vertical fluorescence was detected (I_{vv}).Secondly, the vertical excitation light was selected, and the horizontal fluorescence was detected (I_{vh}). Thirdly, horizontal excitation light was selected and fluorescence in the horizontal direction was detected (I_{hh}).Last, the excitation light in the horizontal direction was selected and fluorescence in the vertical direction was detected (I_{hv}). Each plot represents the average of three measurements. This measurement was performed at least three times for each condition. The excited wavelength was λ_{ex}=357 nm, and the fluorescence intensity was monitored at λ_{em}=430nm. Anisotropy values r was calculated as,

$$r = \frac{I_{VV} - G I_{VH}}{(I_{VV} - G I_{VH})}$$

G is the correction factor, $G = \frac{I_{HV}}{I_{HH}}$ and need to calculate for each sample.

Lipid membrane order can be discussed using r obtained by the above equation. Higher values of *r* indicate a more ordered state of the bilayer.

3-2-11 Aβ protofibril preparation

Aβ protofibril was prepared by using the same method as in the previous studies(Hamada et al., 2010; Morita et al., 2012; Phan et al., 2014). Aβ and Aβ-488 were dissolved in ammonia aq to 200 μM and stored at -80℃. Aβ and Aβ-488 were mixed in a ratio of 2:1 and diluted to 80μM with Tris-HCL buffer (20mM, pH 7.4). The diluted Aβ mixture was incubated for 12 hrs at 37℃ to form Aβ protofibril (Fig. 3-8). Aβ protofibril (80μM) was diluted with the GUV solution to 5 μM and. We prepared an observing chamber using the liposomal solution containing Aβ protofibril and observed them with a confocal laser scanning microscopy (FV-1000, Olympus, Tokyo, Japan) for less than 90 sec.

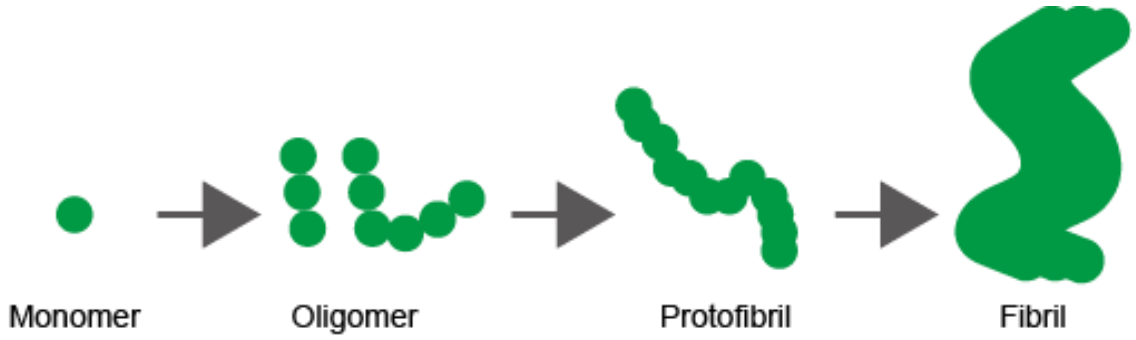

Fig. 3-8 Schematic of Aβ protofibril preparation

3-3 Results

3-3-1 The effect of Toc and Toc3 on the L_o/L_d phase separation

To understand the effect of Toc and Toc3 on the L_o/L_d phase separated GUVs, raft mimicking GUVs composed of DOPC/DPPC/ Chol (=40: 40: 20) and 0~10% Toc or Toc3 were observed using fluorescence microscopy at room temperature. We used Rhodamine-DHPE for staining L_d phase. L_o phase is a dark circular region rich in DPPC and Chol. As previously reported, The GUVs without VE showed L_o /L_d phase separation (Fig. 3-9 (a)). Then, we added Toc or Toc3 before hydration and prepared raft mimicking GUVs. Raft mimicking GUVs containing 5% or 10% VE also showed L_o/ L_d phase separation and did not affect the fraction of phase separated GUVs (Fig. 3-9 (b)). These data suggest that VEs do not affect the L_o/ L_d phase separation at room temperature. To further understand the effect of VEs (Toc and Toc3) on the L_o phase formation, we measured the miscibility temperature T_{mix} of L_o/L_d phase separate GUVs. Raft mimicking GUVs were observed under temperature control. We counted more than 60 GUVs and measured the fraction of phase separated GUVs at each temperature. At lower temperatures, GUVs often showed L_o/ L_d phase separation, whereas at higher temperatures, L_o phase often disappeared. Without VEs, T_{mix} was 35.7℃. Next, Toc and Toc3 were added to ternary GUVs and measure T_{mix}. Addition of Toc or Toc3 resulted in a T_{mix} of 35.8℃(5% Toc), 35.1℃(10% Toc), 35.1℃(5% Toc3), and 35.7℃(10% Toc3) for the L_o phase, respectively. T_{mix} was not affected by Toc and Toc3(Fig. 3-9 (c, d)).

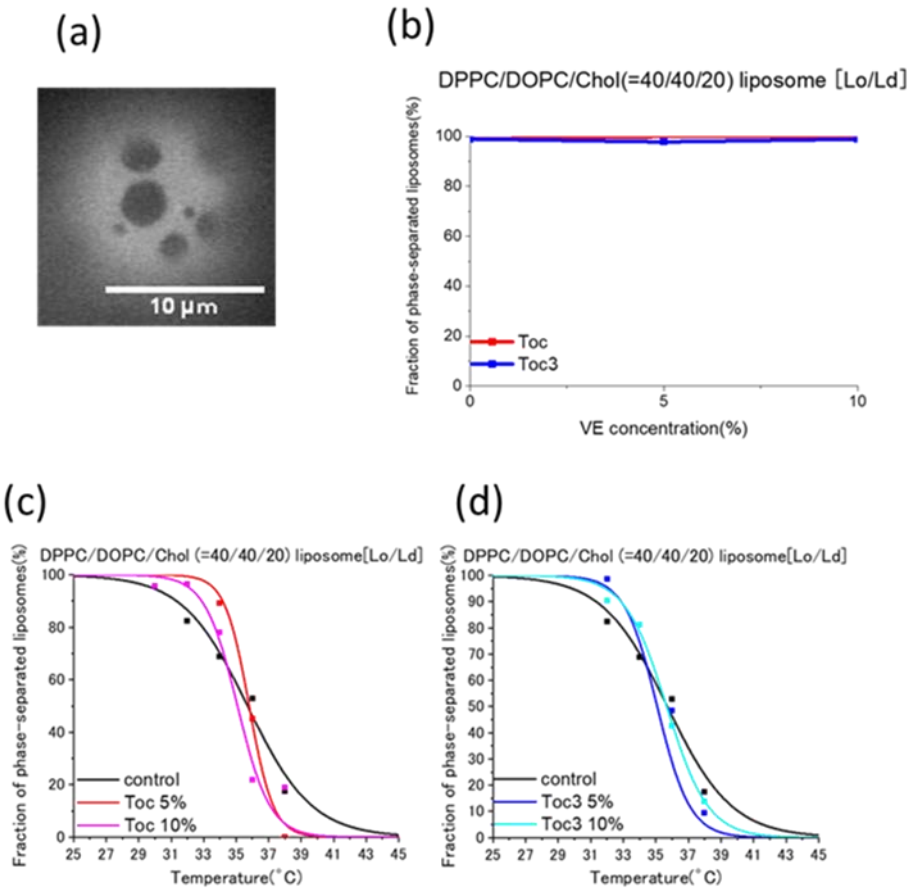

Fig. 3-9 (a) Microscopic images of L_o/L_d phase separation at DOPC/DPPC/Chol=40:40/0 (VE 0%), (b) Fraction of phase-separated GUVs as a function of VE concentration. (c, d) Fraction of phase-separated GUVs containing Toc and Toc3, respectively, as a function of temperature.

3-3-2 DSC measurement in L_o phase mimicking membranes

To quantify the effect of VEs in the thermal stability of L_o phase, DSC was conducted, and T_m was measured (Fig.3-10). MLVs were prepared with/without VEs (Toc and Toc3) 0~10% of the total, while keeping DPPC/Chol=90/10 fixed, and DSC measurements were performed. In this system, we obtained asymmetric thermographs indicative of multiple peaks and heterogeneous distribution of Chol in DPPC membrane(Fig. 3-10 (a, b)). This is consistent with previous work. The previous report has shown that the asymmetric peak can be divided into two peaks. The sharp and broad peaks can be regarded as DPPC-rich S_o phase and a DPPC and Chol-rich L_o phase, respectively(Ko Sugahara et al., 2017). We analyzed the asymmetric thermographs with Origin 2018 and resolved into broad and sharp peaks, which were considered to be the L_o and S_o phases, respectively (Fig. 3-10 (c~f)). Both Toc and Toc3 were found to lower the T_m of the L_o and S_o phases (Fig. 3-10 (g)). Thus, Toc and Toc3 were incorporated into both phases. The T_m of the L_o phase was significantly lower than that of the S_o phase. Furthermore, the T_m of the L_o and S_o phases were significantly lower for Toc3 than for Toc.

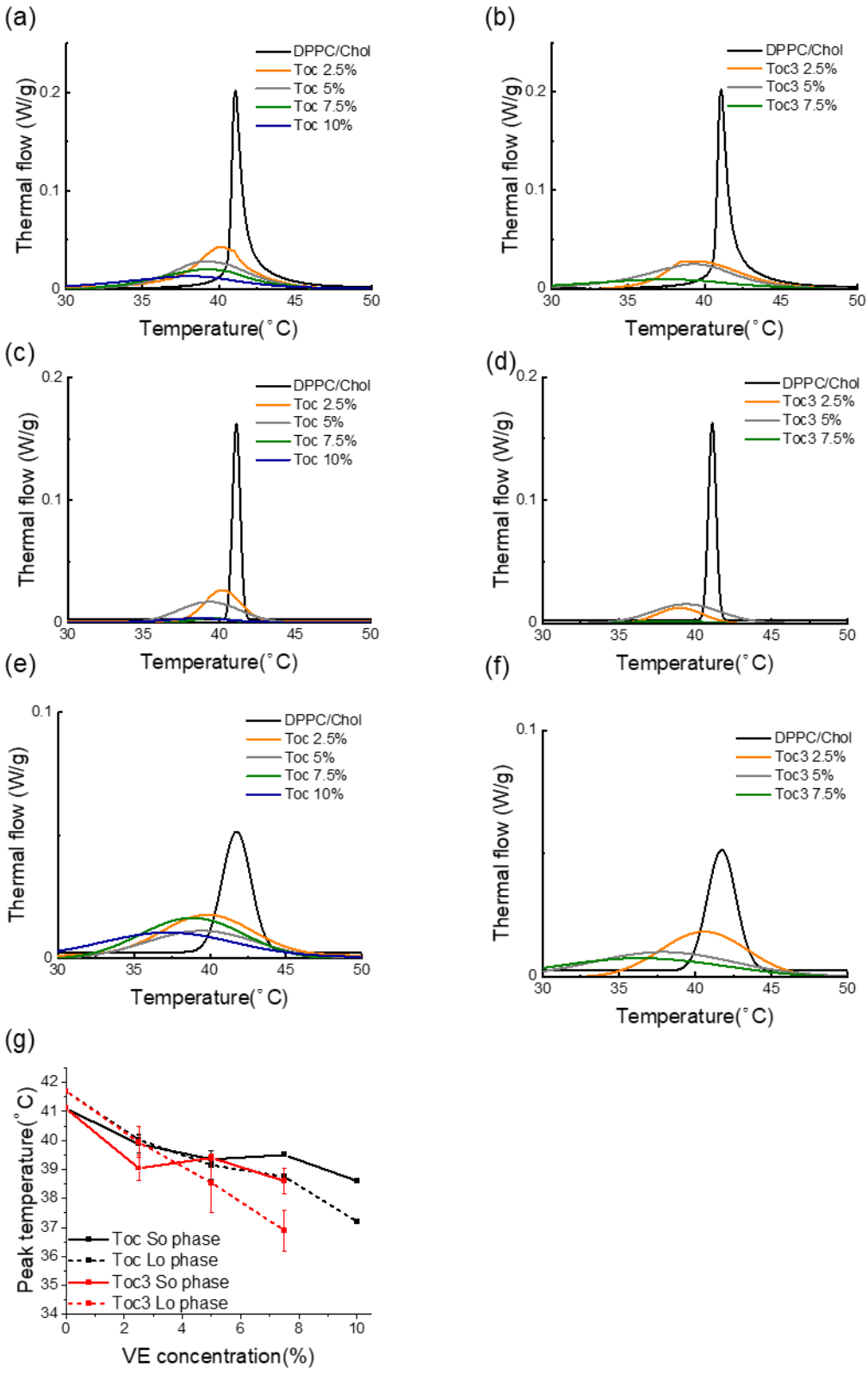
(a)
DPPC/Chol
Toc 2.5%
Toc 5%
Toc 7.5%
Toc 10%
Thermal flow (W/g)
Temperature(˚C)
(b)
DPPC/Chol
Toc3 2.5%
Toc3 5%
Toc3 7.5%
Thermal flow (W/g)
Temperature(˚C)
(c)
DPPC/Chol
Toc 2.5%
Toc 5%
Toc 7.5%
Toc 10%
Thermal flow (W/g)
Temperature(˚C)
(d)
DPPC/Chol
Toc3 2.5%
Toc3 5%
Toc3 7.5%
Thermal flow (W/g)
Temperature(˚C)
(e)
DPPC/Chol
Toc 2.5%
Toc 5%
Toc 7.5%
Toc 10%
Thermal flow (W/g)
Temperature(˚C)
(f)
DPPC/Chol
Toc3 2.5%
Toc3 5%
Toc3 7.5%
Thermal flow (W/g)
Temperature(˚C)
(g)
Toc So phase
Toc Lo phase
Toc3 So phase
Toc3 Lo phase
Peak temperature(˚C)
VE concentration(%)

Fig. 3-10 DSC thermograph of membranes composed of (a)(c)(e)DPPC/Chol (=9/1)/Toc and (b)(d)(f)DPPC/Chol (=9/1)/Toc3. Row data were shown in (a)(b). Deconvoluted data were shown in (c~f). Sharp peaks were shown in (c, d). Broad peaks were shown in (e, f). (g) Peak temperature changes of deconvoluted DSC thermographs as a function of VE concentration.

3-3-3 Line tension of L_o phase boundary in VE containing membranes

The two phase-separated regions have different lipid compositions and therefore different thicknesses; L_d phase is mainly composed of DOPC which has a double bond in the hydrophobic region, forming a thinner region compared to L_o phase, rich in DPPC and Chol. The thickness mismatch is energetically unfavorable because part of the hydrophobic region of DPPC is exposed to water. To reduce that energetic disadvantage, the L_o phase maintains a circular shape, with the shortest boundary interface length. The greater the thickness mismatch between the two phases, the greater the linear tension and the smaller the interfacial fluctuations. On the other hand, if the mismatch between the two is small, the linear tension is small, and the interfacial fluctuations are large.

Line tension is an important indicator of the L_o phase stability. To further gain insights into the effect of Toc and Toc3 on L_o phase, we measured line tension with and without Toc and Toc3. Previous studies showed that Toc decreases the line tension of the L_o phase, by using GUVs containing DOPC/DPPC/Chol (=35/35/30). Without VE, the line tension of L_o phase boundary was 1.89 pN. A previous study showed that line tension of L_o phase boundary was approximately 2 pN(Wongsirojkul et al., 2022). Thus, we regarded this as correct data. Next, we measured the line tension of the L_o phase boundary with Toc and Toc3. Line tension was decreased with Toc and Toc3. The line tension was 1.20pN (5% Toc), 1.43pN (10% Toc), 1.37pN (5% Toc3), 1.14pN (10% Toc3), respectively (Fig. 3-11). These data indicated that VEs decrease L_o phase stability, inconsistent with the data above. The reasons for this are discussed in detail in the discussion section.

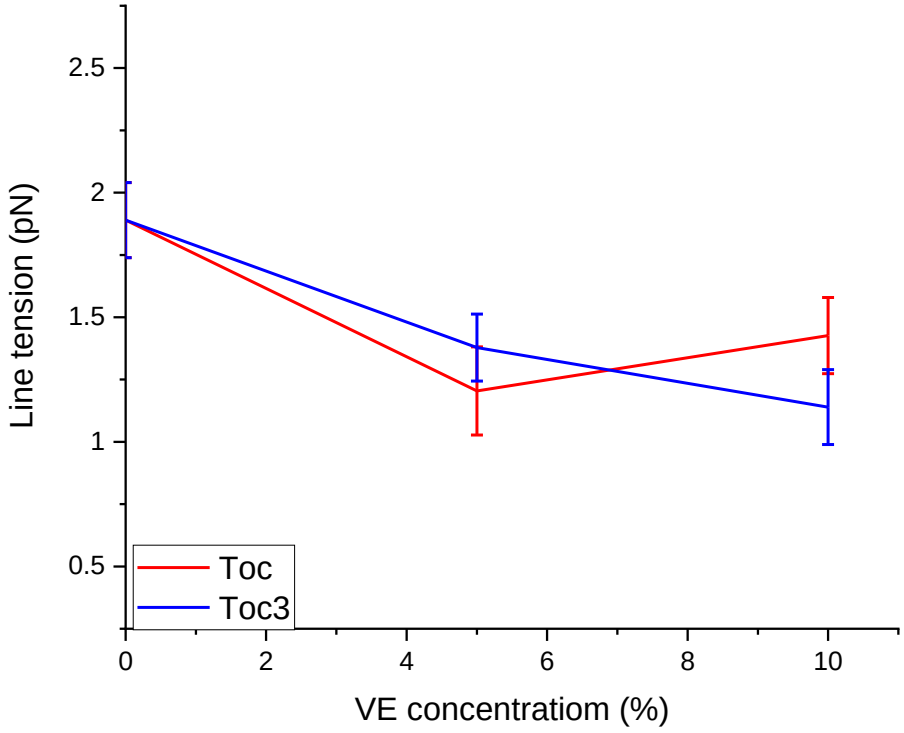

Fig. 3-11 Line tension of L_o phase boundary in the DOPC/DPPC/Chol (=40/40/20) GUVs with/ without Toc and Toc3

3-3-4 DPH anisotropy of DOPC membranes

Although Toc and Toc3 did not affect the formation of L_o domain, Toc and Toc3 decreased line tension. Thus, Toc and Toc3 may incorporate into L_d phase of raft mimicking GUVs and did not affect the L_o/L_d phase separation. However, Toc and Toc3 slightly decreased line tension of L_o domain boundary. We hypothesize that Toc and Toc3 were incorporated into L_d phase and increased L_d phase order. To reveal the effect of Toc and Toc3 on the order of L_d phase, DPH anisotropy was measured using MLVs composed of DOPC with/without VEs (Toc and Toc3) at room temperature. Toc and Toc3 increased the DPH anisotropy of DOPC, indicative of increasing membrane order (Fig. 3-12). We cannot detect the difference between Toc and Toc3 on membrane order.

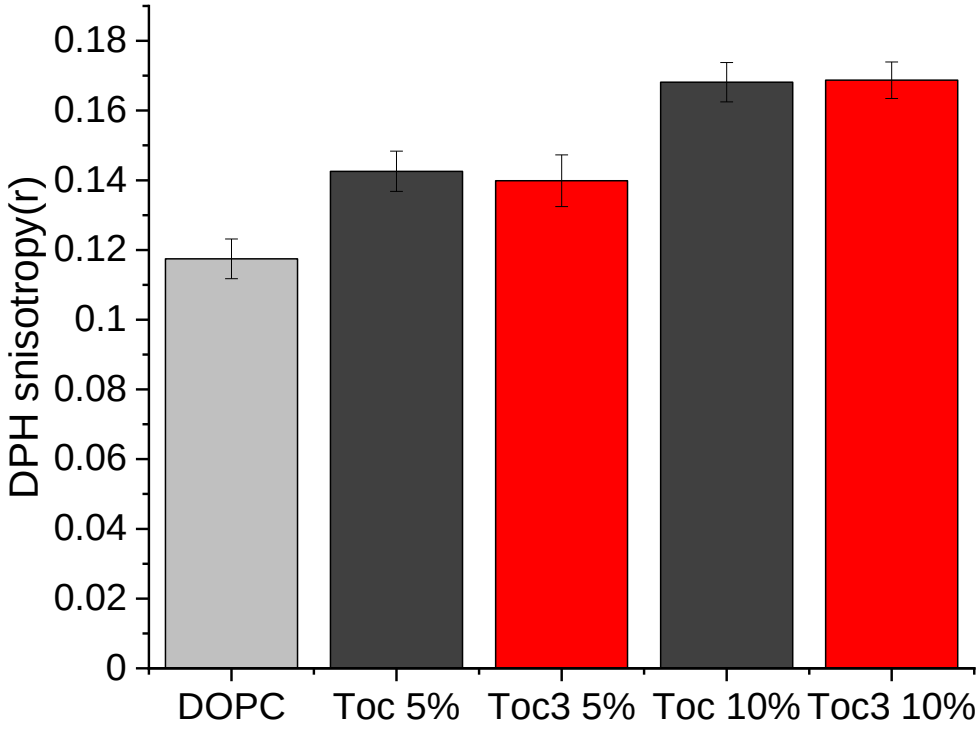

Fig. 3-12 Mean DPH anisotropy (r) in MLVs composed of DOPC/Toc and DOPC/Toc3. These measurements were conducted at room temperature.

3-3-5 Observation of ER mimicking membranes containing Toc and Toc3

To understand the effect of Toc and Toc3 on the S_o phase. Toc and Toc3 were hydrophobic, and they were incorporated into ER mimicking GUVs. We made ER mimicking GUVs composed of DOPC/DPPC (=50: 50) and 0~10% Toc or Toc3 and observed them using fluorescent microscopy at room temperature.ER mimicking GUVs containing 0% VE showed non-circular domain which indicate that the domain was not liquid phase but solid phase (Fig. 3-13 (a)). This domain structure was consistent with previous works. ER mimicking GUVs containing 3 and 5% Toc and Toc3 showed domain shrink, not showing domain disappearance (Fig. 3-13 (b, c)). ER mimicking GUVs containing 8% and 10% Toc and Toc3 destabilize S_o phase and showed a heterogeneous phase (Fig. 3-13 (d)). Unlike previous studies which reported more effect of Ton3 on membrane property than Toc, Toc3 had stronger effect on S_o phase formation (Fig. 3-13 (e)).

Next, to investigate the effect of phase-separated structure on thermal stability, microscopic observations were made during temperature change to determine the phase-separation ratio. First, ER mimicking GUVs were prepared from a DPPC/DOPC=50/50 lipid solution and the T_{mix} of the S_o phase was determined; the T_{mix} of the S_o phase without VE was 37.8°C (Fig. 3-13(f, g). Then, the DPPC/DOPC = 50/50 ratio was fixed, and Toc or Toc3 was added to make GUVs at 5% and 10%. The T_{mix} of the S_o phase was determined under each condition by fluorescence microscopy. Addition of Toc or Toc3 resulted in a T_{mix} of 34.9°C (5% Toc), 21.3℃ (10% Toc), 36.5°C (5% Toc3), and 23.4℃ (10% Toc3) for the S_o phase, respectively. In both cases, the T_{mix} was lower than that of

the control.

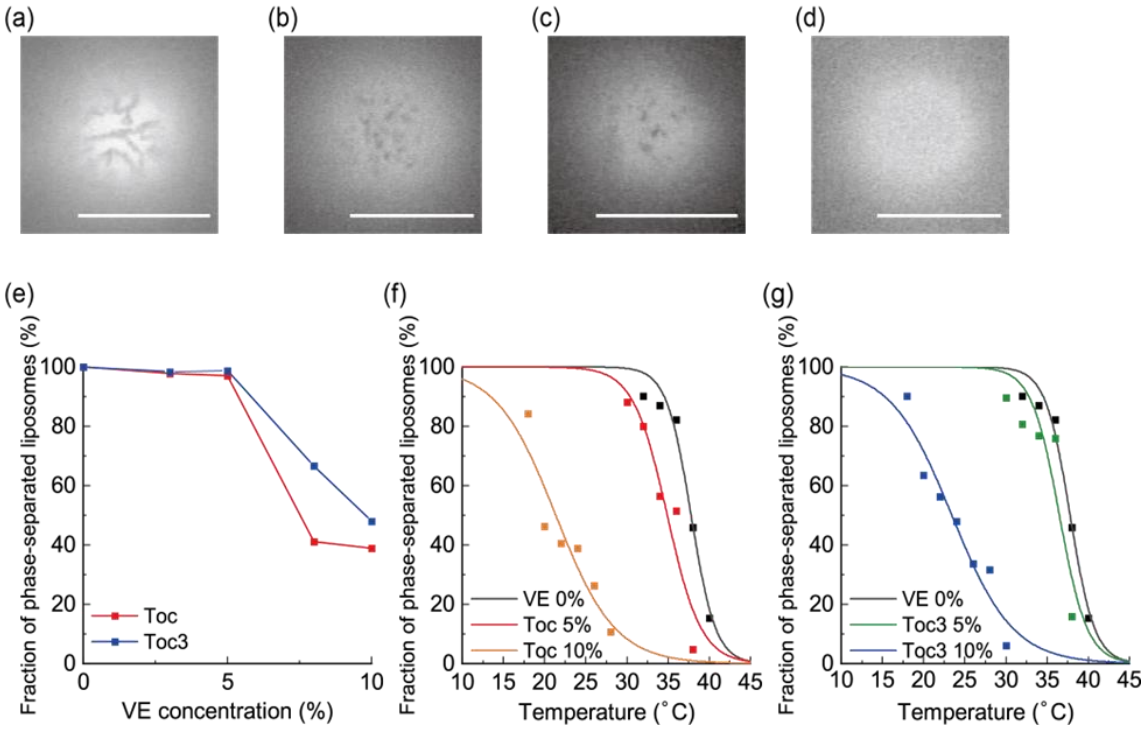

Fig. 3-13 (a) Microscopic images of S_o/L_d phase separation at DOPC/DPPC=50:50 (VE 0%), (b) at DOPC/DPPC/Toc=47.5:47.5:5 (Toc 5%), and (c) at DOPC/DPPC/Toc3=47.5:47.5:5 (Toc3 5%). (d) Microscopic image of homogeneous GUVs at DOPC/DPPC/Toc=45:45:10 (Toc 10%). Scale bars are 10 μm. (e) Fraction of phase-separated GUVs as a function of VE concentration. (f, g) Fraction of phase-separated GUVs containing Toc and Toc3, respectively, as a function of temperature.

3-3-6 DSC measurement for S_o phase mimicking membrane containing Toc and Toc3

Next, we investigated the effect of Toc and Toc on DPPC intermolecular interactions by adding 0-10% of Toc or Toc3 to the DPPC solution, making MLV, and performing DSC measurements. The peak temperature represents the phase transition of DPPC from the gel phase to the liquid crystal phase. In the case of Toc containing MLV, the peak temperature shifted to the lower temperature as shown in the previous literature (Fig. 3-14 (a))(Neunert et al., 2018). We showed that Toc3 also lowers the peak temperature (Fig. 3-14 (b). Therefore, the peak shift by Toc and Toc3 indicates that Toc and Toc3 were incorporated into DPPC membranes and the intermolecular interaction of DPPC is weakened and destabilized.

Furthermore, we found that VE containing thermograph was asymmetric, indicative of containing multiple peaks and heterogeneous distribution of Toc and Toc3 in DPPC membranes (Fig. 3-14 (a, b)). The thermograph without VE is sharp and symmetrical in shape. We analyzed the thermograph and found two peak, sharp peaks and broad peak (Fig. 3-14 (c~f)). The sharp peak at higher temperatures and the broad peak at lower temperatures corresponded to the VE-poor S_o phase and VE-rich S_o phase, respectively. These two peaks shifted toward a lower temperature as the concentration of VE increased (Fig, 3-14 (c~f)). As previously reported, Toc showed a concentration-dependent decrease in the phase transition temperature of DPPC(Neunert et al., 2018). In this study, we found that Toc3 slightly destabilized these phases compared with Toc. Therefore, VE reduced the thermal stability of both phases.

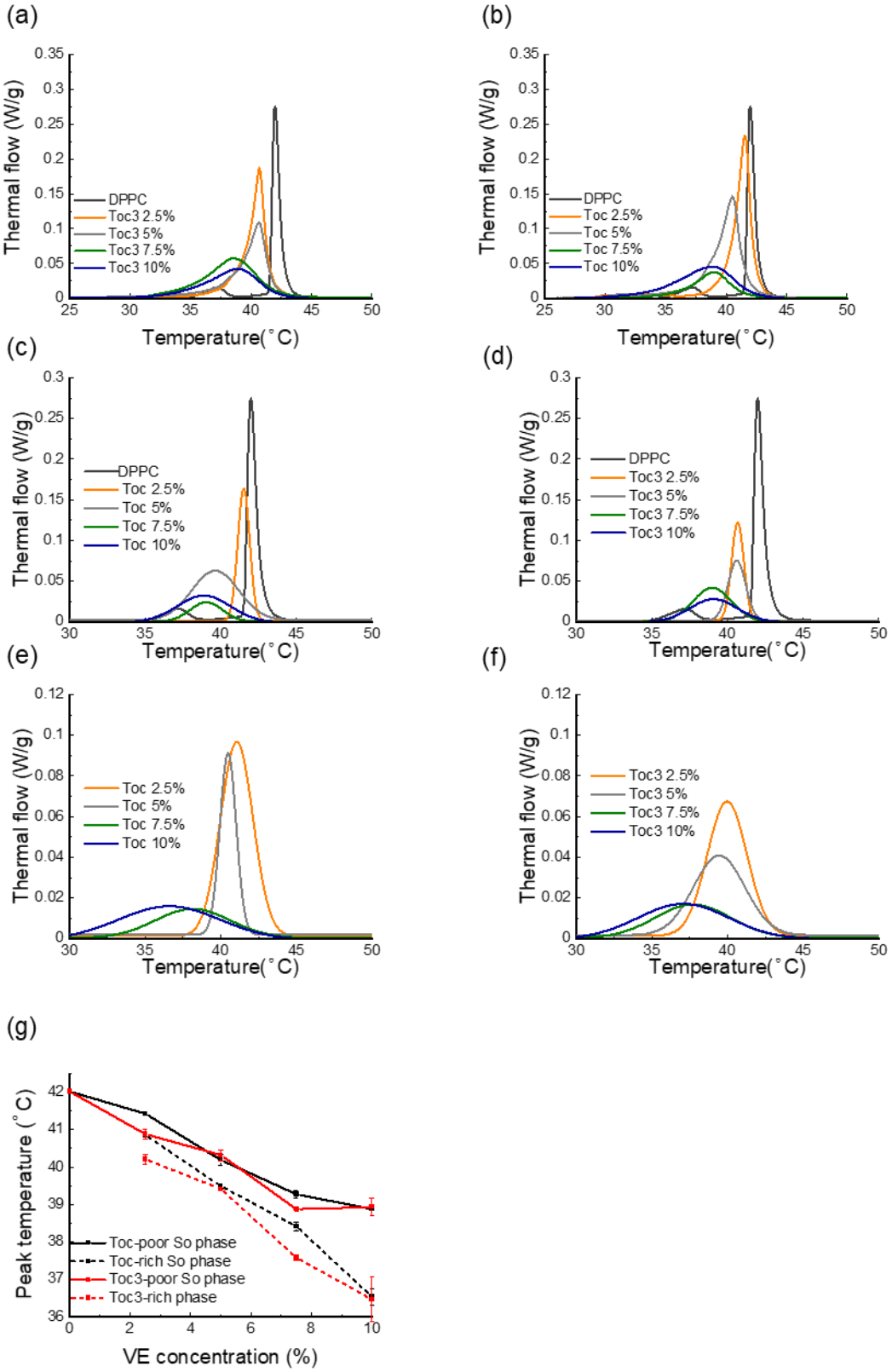
(a)
Thermal flow (W/g)
Temperature(˚C)
DPPC
Toc3 2.5%
Toc3 5%
Toc3 7.5%
Toc3 10%
(b)
Thermal flow (W/g)
Temperature(˚C)
DPPC
Toc 2.5%
Toc 5%
Toc 7.5%
Toc 10%
(c)
Thermal flow (W/g)
Temperature(˚C)
DPPC
Toc 2.5%
Toc 5%
Toc 7.5%
Toc 10%
(d)
Thermal flow (W/g)
Temperature(˚C)
DPPC
Toc3 2.5%
Toc3 5%
Toc3 7.5%
Toc3 10%
(e)
Thermal flow (W/g)
Temperature(˚C)
Toc 2.5%
Toc 5%
Toc 7.5%
Toc 10%
(f)
Thermal flow (W/g)
Temperature(˚C)
Toc3 2.5%
Toc3 5%
Toc3 7.5%
Toc3 10%
(g)
Peak temperature (˚C)
VE concentration (%)
Toc-poor So phase
Toc-rich So phase
Toc3-poor So phase
Toc3-rich phase

Fig. 3-14 DSC thermograph of membranes composed of (a)(c)(e)DPPC/Toc and (b)(d)(f)DPPC/Toc3. Row data were shown in (a)(d). Deconvoluted data were shown in (b, c, e, f). Sharp peaks were shown in (b, e). Broad peaks were shown in (c, f). (g) Peak temperature changes of deconvoluted DSC thermographs as a function of VE concentration.

3-3-7 Adsorption of Aβ on ER-mimicking membrane containing Toc and Toc3

Next, we added Aβ protofibril to ER mimicking GUVs containing Toc and Toc3 and observed them at room temperature by confocal laser scanning microscopy. We used Aβ peptide with 42 amino acid residues and fluorescence-labeled Aβ (Hylite Fluor 488, Aβ-488) and mixed them at a ratio of 2:1. The mixed Aβ was incubated for 12 h to spontaneously aggregate into protofibrils(Morita et al., 2012). The detailed sample preparation can be found in the supporting information. At VE 0%, the S_o/L_d phase-separated GUVs were found and the regions with higher and lower Rhod-DHPE fluorescence intensities correspond to the L_d and S_o phases, respectively. The fluorescence intensity of Aβ-488 was higher in the S_o phase. This indicated that Aβ protofibril selectively adsorbed onto the S_o phase and this result is consistent with some previous studies (Fig. 3-14 (a))(Hamada et al., 2010; Morita et al., 2012; Phan et al., 2014). On the other hand, at VE 10%, half of the GUVs exhibited the homogeneous phase as we have already mentioned in Fig. 3-14 (b, c). In such ER mimicking GUVs, we could not observe the Aβ adsorption onto the surface of GUVs. We concluded that the Aβ adsorption correlated with the S_o phase formation. Since Toc strongly suppressed the formation of the S_o phase than Toc3 from microscopic observation, Toc prevented the Aβ adsorption onto the ER-mimicking membranes than Toc3.

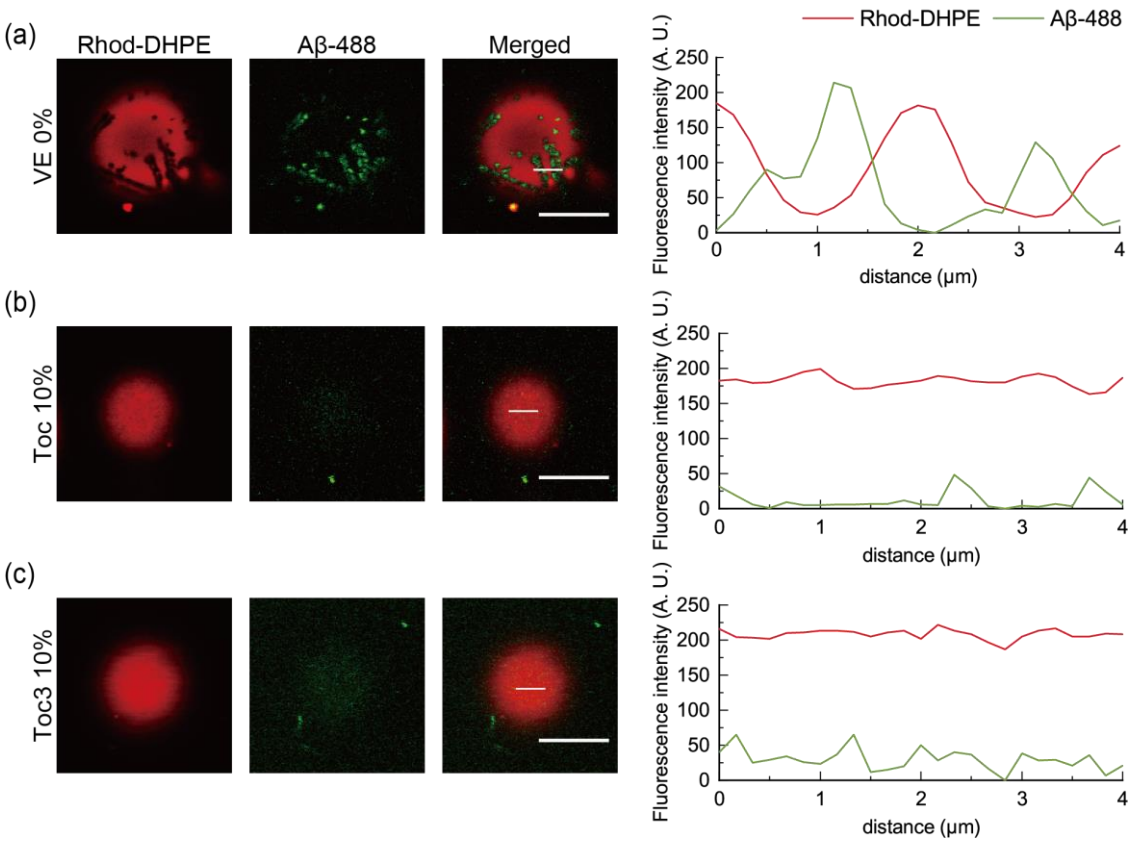

Fig. 3-15 Microscopic images obtained by confocal laser scanning microscopy and fluorescence intensity profiles along the white lines in merged images. Aβ protofibril absorption onto GUVs containing (a)VE 0%; (b)Toc 10%; (c)Toc3 10%. Red and green fluorescence represent Rhod-DHPE and Aβ-488, respectively. Red and green lines in the fluorescence intensity profiles indicate the intensities of Rhod-DHPE and Aβ-488, respectively. Scale bars are 10μm.

3-4 Discussion

3-4-1 Distribution of VE in L_o/L_d phase separated membrane

No effect of VE on L_o/L_d phase separationwas found in the raft model. From the DSC results, if VE distributes to the L_o phase, it inhibits L_o phase formation and causes a decrease in the fraction of phase separationed GUVs and T_{mix}. Thus, VE is considered to be partitioned into the L_d phase. This result differs from previous results(DiPasquale et al., 2020; Muddana et al., 2012). Some reports showed that VE inhibits L_o phase formation. A possible reason for the difference from the present study may be due to the different lipid composition in GUVs. In previous reports, DOPC/DPPC/Chol is 37.5/37.5/25, 1/1/0.7. Therefore, compared to the present experimental system (40/40/20), proportion of the L_d phase is small and the capacity for VE entry is reduced. As a result, VE is more likely to be distributed to the L_o phase and the L_o phase is more easily destabilized. VE slightly decreased the line tension of the L_o phase boundary. DPH experiments showed that VE increases the membrane order in the L_d phase. Therefore, for L_o/L_d GUVs, VE may distribute to the L_d phase, increasing membrane order and thus decreasing the line tension of the L_o phase boundary. The reason why no difference was observed between Toc and Toc3 is suggested by the fact that they exhibit the same behavior in this model membrane.

3-4-2 Distribution of VE in S_o/L_d phase separated membrane

Since both Toc and Toc3 decreased the thermal stability of DPPC membranes representing the S_o phase in the DSC measurements, they may be mainly partitioned into L_d phase in the S_o/L_d phase-separated membranes. However, some amount of VE was incorporated into DPPC-rich S_o phase owing to mixing entropy. We considered that the amount of Toc in S_o phase was larger than that of Toc3, since Toc3 destabilized DPPC membranes than Toc from the DSC measurements. On the other hand, Toc destabilized the phase-separated structures at room temperature and decreased T_{mix} as compared to Toc3. VE incorporated into the S_o phase diluted the favorable interaction between DPPC molecules and decreased T_{mix}(Allender and Schick, 2017). The effect of destabilization of by Toc was stronger than Toc3, since the amount of Toc in the S_o phase was larger. In future, it is important to measure the exact amount of VE in S_o phase by some experiments such as nuclear magnetic resonance (NMR).

The difference of partitioning between Toc and Toc3 arose from the chemical structure difference. From normal-phase high-performance liquid chromatography (HPLC), it was reported that Toc3 with the unsaturation side chain is more polar than Toc(Kamal-Eldin et al., 2000). In other words, Toc3 is more hydrophilic than Toc. The DOPC-rich L_d phase is loosely packed than the DPPC-rich S_o phase, making it easier to incorporate water molecules into the L_d phase. Therefore, Toc3 is more likely to be partitioned into the hydrophilic-L_d phase than Toc. In contrast, the amount of Toc in the S_o phase became larger than that of Toc3. Similar behavior has been observed with the addition of fatty acids to lipid membranes, and a saturated fatty acid (palmitic acid) has higher affinity to the S_o phase than a trans-fatty acid (elaidic acid)(Shimokawa et al., 2017).

3-4-3 VE and 24S-OHC induced ER stress

There are various conflicting reports regarding Toc and Toc3(Boccardi et al., 2016; Sen et al., 2006). The chromanone ring structure responsible for the antioxidant effect is the same, and only the hydrocarbon chains are different between them. This may result in their different localization in organelle membranes and membrane subdomains and then, cause a different effect on diseases. In this study, we found that Toc inhibits S_o phase formation more strongly than Toc3. This suggests that local lipid composition affects the localization of Toc and Toc3. We have shown that 25(S)-hydroxycholesterol (25S-OHC) induces ER stress-induced cell death via changes in membrane properties(Sharma et al., 2017). 24S-OHC, which has a similar structure to 25S-OHC, also induces neuronal cell death via ER stress(Urano et al., 2019). Toc can inhibit this 24S-OHC induced cell death(Kimura et al., 2018). However, the mechanism by which Toc inhibits cytotoxicity by 24S-OHC is poorly understood. 24S-OHC is esterified by acyl-coenzyme A: cholesterol acyltransferases (ACAT1) residing at ER membrane protein, to form 24S-OHC-ester, which causes loss of the ER membrane integrity(Urano et al., 2019). Our study suggests that Toc has a greater effect on ER membrane properties than Toc3, and that the change in ER membrane properties by Toc may contribute to the mitigation of the toxicity of 24S-OHC ester.

3-4-4 S_o phase formation and ER stress-related diseases

ER is one of the most important organelles for lipid metabolism, and ER membrane changes its membrane lipidome in response to the surrounding environment. Supplementation of cultured cells with saturated fatty acids promotes synthesis of saturated lipids in ER, leading to the formation of S_o phase(Shen et al., 2017). The formation of the S_o phase may be involved in physiological responses inside and outside the ER. First, our results suggest that denatured proteins and endocytosis-incorporated Aβ protofibril adsorption to the S_o phase in the ER lumen. This may allow them to escape degradation by the ubiquitin-proteasome pathway and disrupt proteostasis.

VE is expected to be effective in inhibiting the onset of AD(Browne et al., 2019; Mangialasche et al., 2010; Nishida et al., 2009). However, it is not clear whether Toc or Toc3 is more effective in inhibiting AD. One of the reasons for this is that there are multiple mechanisms involved in the pathogenesis of AD. Using an ER-mimicking membrane, our results have clearly show that Toc and Toc3 inhibit adsorption of Aβ protofibril on S_o phase(Fig. 3-16). Furthermore, Toc is more effective than Toc3. This is because Toc destabilizes the S_o domain more strongly than Toc3, and a similar mechanism may apply to other molecules such as docosahexaenoic acid (DHA) and eicosatetraenoic acid (EPA), which are thought to prevent Alzheimer's disease[29–31].

The involvement of ER stress has been reported in diseases other than AD. Diabetes is one such example(Huang et al., 2007). VE as well as DHA is thought to be related to the development of type 2 diabetes(Badawi, 2011; De Caterina et al., 2007). Saturated

fatty acid intake is known to be a risk for diabetes(Risérus et al., 2009). DHA is known to alter cell lipidome and increases polyunsaturated lipids(Levental et al., 2020). Since the formation of phase-separated structures is influenced by lipid composition, the formation of lipids with low T_m, such as polyunsaturated lipids, may contribute in an inhibitory manner to S_o phase formation in the ER membrane(Veatch and Keller, 2003). Thus, preventing saturation of ER membrane lipids can avoid UPR and cell death and alleviate these diseases.

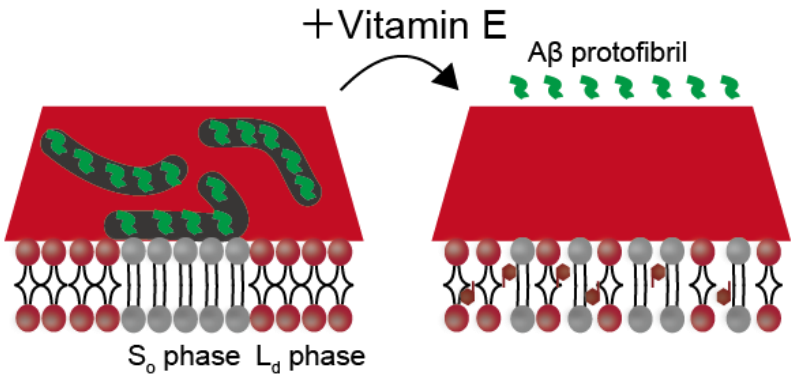

Fig. 3-16 Scheme of Aβ protofibril adsorption onto S_o phase

Chapter 4
General Conclusion

4-1 General Conclusion

In this study, we analyzed by the three-dimensional membrane behavior induced by surfactants (Chapter 2) and the effects of α-Toc and α-Toc3 on phase separation and the membrane adsorption of Aβ (Chapter 3), by using liposomes.

In Chapter 2, GUVs consisting of DOPC were prepared and membrane dynamics induced by surfactant addition were observed. Based on the membrane dynamics, we compared the irritation classification with that of previous studies and predicted the irritancy. The results showed that the amino acid surfactant, sodium lauroyl glutamate, increased the excess surface area of the membrane and then the dynamics stopped. Although this irritancy is unclassified, its behavior is like that of hyperirritant dynamics, suggesting that it is a strong irritant. This result agrees with the results of human studies. Dynamics were also examined with a mixture of sodium lauroyl glutamate and an amphoteric surfactant, either cocamidopropyl betaine or lauramidopropyl betaine. Both were found to decrease the irritancy of sodium lauroyl glutamate. Surprisingly, even in the mixed system, there was a correlation between the irritation classification by membrane dynamics and the results of the human stinging test.

From fluorescence experiment, Lipid transfer between membrane bilayers under conditions with the addition of the nonionic surfactant tween 20 showed an increase in $V_{Flip\text{-}flop}$ as the concentration was increased. This suggests that the entry of surfactant into the membrane increases $V_{Flip\text{-}Flop}$ and affects the dynamics of the membrane, such as an increase in excess membrane area and shrinkage.

In Chapter 3, liposomes consisting of DOPC/DPPC/Chol = (40/40/20 or 50/50/0) were

prepared, which the L_o phase or S_o phase coexisted with the L_d phase, raft and ER membrane mimicking GUV, respectively. Microscopic observation showed that Toc and Toc3 did not affect the formation rate of L_o/L_d phase separation in GUVs. However, both Toc and Toc3 slightly decreased the line tension at the L_o/L_d boundary. The DSC results showed that both Toc and Toc3 had low affinity to Chol. This suggested that Toc and Toc3 are easily partitioned to L_d. Next, we investigated the effects of Toc and Toc3 on the L_d phase using DPH and found that both Toc and Toc3 increase the order. Therefore, Toc and Toc3 may distribute to the L_d phase of L_o/L_d and increase the membrane order, thereby slightly reducing the mismatch between L_o and L_d thicknesses and the line tension.

We investigated the phase behavior and thermal stability of the phase-separated structures in S_o/L_d GUV containing Toc and Toc3. From microscopic observations, Toc suppressed S_o phase formation in S_o/L_d GUV more strongly than Toc3. On the other hand, DSC showed that the DPPC-rich S_o phase was destabilized more by Toc3 than by Toc. It was also demonstrated that the amount of Toc in the S_o phase was larger than that of Toc3, and Toc inhibited the formation of the S_o phase more strongly than Toc3. In addition, Aβ protofibril adsorption onto S_o/L_d GUVs were also reduced by VE, especially Toc, due to the suppression of S_o phase formation. It is considered that the suppression of S_o phase formation by adding Toc has more pronounced effects on the reduction of ER stress-denatured proteins compared with the addition of Toc3.

4-2 Future Perspective

We have visualised physiological responses by 2D and 3D membrane dynamics in model membranes. Further detailed analysis is expected in the future.

Recently, several lipid-soluble bioactive molecules have been reported to contribute to physiological responses. The polyunsaturated fatty acid DHA inhibits K-RAS accumulation(Fuentes et al., 2021). In addition, diacylglycerols with different fatty acids accumulates different isoforms(Schuhmacher et al., 2020). A further qualitative analysis of the contribution of these bioactive molecules to the physiological response is expected by studying their effects on membrane dynamics.

In addition, a variety of membrane dynamics were observed in this study. Human studies have shown different results in stimulus evaluation, even within the same dynamics. Therefore, the relationship between the magnitude of membrane dynamics and irritation should also be considered. Future analysis of the magnitude of fine-scale dynamics would allow more detailed stimulus evaluation; AI-based analysis is expected to make this possible.

Membrane dynamics arise in response to changes in a variety of factors, including molecular interactions between membrane lipids and osmotic pressure. Studies of model membranes have analyzed these dynamics physically and mathematically. However, little is known about the relevance of mathematical models to physiological responses. Therefore, the development of mathematical models of membrane dynamics and their application to the understanding of physiological responses will lead to a better understanding and prediction of the functions of bioactive molecules.

In addition, lipidome analysis has recently been active, and it is expected that further

disease-specific lipidome changes will be found in the future. By focusing on changes in lipid composition and adjusting liposome composition, it will be possible to create ageing model liposomes and obesity model liposomes, which will lead to a better understanding of disease pathogenesis.

In this study, an ER stress model was created using amyloid-beta membrane interactions and a pain stimulus model was created using membrane dynamics. In the future, other physiological responses are expected to be modelled using liposomes. For example, temperature-sensitive receptors open and close channels in response to changes in temperature(Kim et al., 2020). Temperature has been reported to affect lipid-lipid interactions and alter membrane properties, which may contribute to heat and cold sensing. In addition, many of the molecules that stimulate olfaction are lipid soluble. Therefore, membrane properties may contribute to the activation of olfactory receptor proteins.

Reference

Adams, C.J., Kopp, M.C., Larburu, N., Nowak, P.R., Ali, M.M.U., 2019. Structure and Molecular Mechanism of ER Stress Signaling by the Unfolded Protein Response Signal Activator IRE1. Front. Mol. Biosci. 6, 11. https://doi.org/10.3389/fmolb.2019.00011

Akbarzadeh, A., Rezaei-Sadabady, R., Davaran, S., Joo, S.W., Zarghami, N., Hanifehpour, Y., Samiei, M., Kouhi, M., Nejati-Koshki, K., 2013. Liposome: classification, preparation, and applications. Nanoscale Res Lett 8, 102. https://doi.org/10.1186/1556-276X-8-102

Allender, D.W., Schick, M., 2017. The Effect of Solutes on the Temperature of Miscibility Transitions in Multicomponent Membranes. Biophysical Journal 113, 1814–1821. https://doi.org/10.1016/j.bpj.2017.08.033

Almanza, A., Carlesso, A., Chintha, C., Creedican, S., Doultsinos, D., Leuzzi, B., Luís, A., McCarthy, N., Montibeller, L., More, S., Papaioannou, A., Püschel, F., Sassano, M.L., Skoko, J., Agostinis, P., de Belleroche, J., Eriksson, L.A., Fulda, S., Gorman, A.M., Healy, S., Kozlov, A., Muñoz-Pinedo, C., Rehm, M., Chevet, E., Samali, A., 2019. Endoplasmic reticulum stress signalling - from basic mechanisms to clinical applications. FEBS J 286, 241–278. https://doi.org/10.1111/febs.14608

Ariyama, H., Kono, N., Matsuda, S., Inoue, T., Arai, H., 2010. Decrease in Membrane Phospholipid Unsaturation Induces Unfolded Protein Response. Journal of Biological Chemistry 285, 22027–22035. https://doi.org/10.1074/jbc.M110.126870

Armstrong, V.T., Brzustowicz, M.R., Wassall, S.R., Jenski, L.J., Stillwell, W., 2003. Rapid flip-flop in polyunsaturated (docosahexaenoate) phospholipid membranes. Archives of Biochemistry and Biophysics 414, 74–82. https://doi.org/10.1016/S0003-9861(03)00159-0

Badawi, A., 2011. Vitamins D, C, and E in the prevention of type 2 diabetes mellitus: modulation of inflammation and oxidative stress. BTT 5, 7–19. https://doi.org/10.2147/BTT.S14417

Bagga, D., Wang, L., Farias-Eisner, R., Glaspy, J.A., Reddy, S.T., 2003. Differential effects of prostaglandin derived from ω-6 and ω-3 polyunsaturated fatty acids on COX-2 expression and IL-6 secretion. Proc. Natl. Acad. Sci. U.S.A. 100, 1751–1756. https://doi.org/10.1073/pnas.0334211100

Boccardi, V., Baroni, M., Mangialasche, F., Mecocci, P., 2016. Vitamin E family: Role in the pathogenesis and treatment of Alzheimer's disease. Alzheimer's & Dementia:

Translational Research & Clinical Interventions 2, 182–191. https://doi.org/10.1016/j.trci.2016.08.002

Brown, D.A., Rose, J.K., 1992. Sorting of GPI-anchored proteins to glycolipid-enriched membrane subdomains during transport to the apical cell surface. Cell 68, 533–544. https://doi.org/10.1016/0092-8674(92)90189-J

Browne, D., McGuinness, B., Woodside, J.V., McKay, G.J., 2019. Vitamin E and Alzheimer's disease: what do we know so far? CIA Volume 14, 1303–1317. https://doi.org/10.2147/CIA.S186760

Burgos, R.A., Conejeros, I., Hidalgo, M.A., Werling, D., Hermosilla, C., 2011. Calcium influx, a new potential therapeutic target in the control of neutrophil-dependent inflammatory diseases in bovines. Veterinary Immunology and Immunopathology 143, 1–10. https://doi.org/10.1016/j.vetimm.2011.05.037

Capolupo, L., Khven, I., Lederer, A.R., Mazzeo, L., Glousker, G., Ho, S., Russo, F., Montoya, J.P., Bhandari, D.R., Bowman, A.P., Ellis, S.R., Guiet, R., Burri, O., Detzner, J., Muthing, J., Homicsko, K., Kuonen, F., Gilliet, M., Spengler, B., Heeren, R.M.A., Dotto, G.P., La Manno, G., D'Angelo, G., 2022. Sphingolipids control dermal fibroblast heterogeneity. Science 376, eabh1623. https://doi.org/10.1126/science.abh1623

Conquer, J.A., Tierney, M.C., Zecevic, J., Bettger, W.J., Fisher, R.H., 2000. Fatty acid analysis of blood plasma of patients with alzheimer's disease, other types of dementia, and cognitive impairment. Lipids 35, 1305–1312. https://doi.org/10.1007/s11745-000-0646-3

Dalal, P.J., Muller, W.A., Sullivan, D.P., 2020. Endothelial Cell Calcium Signaling during Barrier Function and Inflammation. The American Journal of Pathology 190, 535–542. https://doi.org/10.1016/j.ajpath.2019.11.004

De Caterina, R., Madonna, R., Bertolotto, A., Schmidt, E.B., 2007. n-3 Fatty Acids in the Treatment of Diabetic Patients: Biological rationale and clinical data. Diabetes Care 30, 1012–1026. https://doi.org/10.2337/dc06-1332

DiPasquale, M., Nguyen, M.H.L., Rickeard, B.W., Cesca, N., Tannous, C., Castillo, S.R., Katsaras, J., Kelley, E.G., Heberle, F.A., Marquardt, D., 2020. The antioxidant vitamin E as a membrane raft modulator: Tocopherols do not abolish lipid domains. Biochimica et Biophysica Acta (BBA) - Biomembranes 1862, 183189. https://doi.org/10.1016/j.bbamem.2020.183189

Esposito, C., Tian, A., Melamed, S., Johnson, C., Tee, S.-Y., Baumgart, T., 2007. Flicker Spectroscopy of Thermal Lipid Bilayer Domain Boundary Fluctuations. Biophysical Journal 93, 3169–3181. https://doi.org/10.1529/biophysj.107.111922

Evans, H.M., Bishop, K.S., 1922. On the Existence of a Hitherto Unrecognized Dietary Factor Essential for Reproduction. Science 56, 650–651. https://doi.org/10.1126/science.56.1458.650

Fanning, S., Haque, A., Imberdis, T., Baru, V., Barrasa, M.I., Nuber, S., Termine, D., Ramalingam, N., Ho, G.P.H., Noble, T., Sandoe, J., Lou, Y., Landgraf, D., Freyzon, Y., Newby, G., Soldner, F., Terry-Kantor, E., Kim, T.-E., Hofbauer, H.F., Becuwe, M., Jaenisch, R., Pincus, D., Clish, C.B., Walther, T.C., Farese, R.V., Srinivasan, S., Welte, M.A., Kohlwein, S.D., Dettmer, U., Lindquist, S., Selkoe, D., 2019. Lipidomic Analysis of α-Synuclein Neurotoxicity Identifies Stearoyl CoA Desaturase as a Target for Parkinson Treatment. Molecular Cell 73, 1001-1014.e8. https://doi.org/10.1016/j.molcel.2018.11.028

Fuentes, N.R., Mlih, M., Wang, X., Webster, G., Cortes-Acosta, S., Salinas, M.L., Corbin, I.R., Karpac, J., Chapkin, R.S., 2021. Membrane therapy using DHA suppresses epidermal growth factor receptor signaling by disrupting nanocluster formation. Journal of Lipid Research 62, 100026. https://doi.org/10.1016/j.jlr.2021.100026

Funk, C.D., 2001. Prostaglandins and Leukotrienes: Advances in Eicosanoid Biology. Science 294, 1871–1875. https://doi.org/10.1126/science.294.5548.1871

Galluzzi, L., Vitale, I., Aaronson, S.A., Abrams, J.M., Adam, D., Agostinis, P., Alnemri, E.S., Altucci, L., Amelio, I., Andrews, D.W., Annicchiarico-Petruzzelli, M., Antonov, A.V., Arama, E., Baehrecke, E.H., Barlev, N.A., Bazan, N.G., Bernassola, F., Bertrand, M.J.M., Bianchi, K., Blagosklonny, M.V., Blomgren, K., Borner, C., Boya, P., Brenner, C., Campanella, M., Candi, E., Carmona-Gutierrez, D., Cecconi, F., Chan, F.K.-M., Chandel, N.S., Cheng, E.H., Chipuk, J.E., Cidlowski, J.A., Ciechanover, A., Cohen, G.M., Conrad, M., Cubillos-Ruiz, J.R., Czabotar, P.E., D'Angiolella, V., Dawson, T.M., Dawson, V.L., De Laurenzi, V., De Maria, R., Debatin, K.-M., DeBerardinis, R.J., Deshmukh, M., Di Daniele, N., Di Virgilio, F., Dixit, V.M., Dixon, S.J., Duckett, C.S., Dynlacht, B.D., El-Deiry, W.S., Elrod, J.W., Fimia, G.M., Fulda, S., García-Sáez, A.J., Garg, A.D., Garrido, C., Gavathiotis, E., Golstein, P., Gottlieb, E., Green, D.R., Greene, L.A., Gronemeyer, H., Gross, A., Hajnoczky, G., Hardwick, J.M., Harris, I.S., Hengartner, M.O., Hetz, C., Ichijo, H., Jäättelä, M., Joseph, B., Jost, P.J., Juin, P.P., Kaiser, W.J., Karin, M., Kaufmann, T., Kepp, O., Kimchi, A., Kitsis, R.N., Klionsky, D.J., Knight, R.A., Kumar, S., Lee, S.W., Lemasters, J.J., Levine, B., Linkermann, A., Lipton, S.A., Lockshin, R.A., López-Otín, C., Lowe, S.W., Luedde, T., Lugli, E., MacFarlane, M., Madeo, F., Malewicz, M., Malorni, W., Manic, G., Marine, J.-C., Martin, S.J., Martinou, J.-C., Medema, J.P., Mehlen, P., Meier, P., Melino, S., Miao, E.A., Molkentin, J.D., Moll, U.M.,

Muñoz-Pinedo, C., Nagata, S., Nuñez, G., Oberst, A., Oren, M., Overholtzer, M., Pagano, M., Panaretakis, T., Pasparakis, M., Penninger, J.M., Pereira, D.M., Pervaiz, S., Peter, M.E., Piacentini, M., Pinton, P., Prehn, J.H.M., Puthalakath, H., Rabinovich, G.A., Rehm, M., Rizzuto, R., Rodrigues, C.M.P., Rubinsztein, D.C., Rudel, T., Ryan, K.M., Sayan, E., Scorrano, L., Shao, F., Shi, Y., Silke, J., Simon, H.-U., Sistigu, A., Stockwell, B.R., Strasser, A., Szabadkai, G., Tait, S.W.G., Tang, D., Tavernarakis, N., Thorburn, A., Tsujimoto, Y., Turk, B., Vanden Berghe, T., Vandenabeele, P., Vander Heiden, M.G., Villunger, A., Virgin, H.W., Vousden, K.H., Vucic, D., Wagner, E.F., Walczak, H., Wallach, D., Wang, Y., Wells, J.A., Wood, W., Yuan, J., Zakeri, Z., Zhivotovsky, B., Zitvogel, L., Melino, G., Kroemer, G., 2018. Molecular mechanisms of cell death: recommendations of the Nomenclature Committee on Cell Death 2018. Cell Death Differ 25, 486–541. https://doi.org/10.1038/s41418-017-0012-4

Guo, J., Ito, H., Higuchi, Y., Bohinc, K., Shimokawa, N., Takagi, M., 2021. Three-Phase Coexistence in Binary Charged Lipid Membranes in a Hypotonic Solution. Langmuir 37, 9683–9693. https://doi.org/10.1021/acs.langmuir.1c00967

Halbleib, K., Pesek, K., Covino, R., Hofbauer, H.F., Wunnicke, D., Hänelt, I., Hummer, G., Ernst, R., 2017. Activation of the Unfolded Protein Response by Lipid Bilayer Stress. Molecular Cell 67, 673-684.e8. https://doi.org/10.1016/j.molcel.2017.06.012

Hamada, T., Hagihara, H., Morita, M., Vestergaard, M.C., Tsujino, Y., Takagi, M., 2012. Physicochemical Profiling of Surfactant-Induced Membrane Dynamics in a Cell-Sized Liposome. J. Phys. Chem. Lett. 3, 430–435. https://doi.org/10.1021/jz2016044

Hamada, T., Morita, M., Kishimoto, Y., Komatsu, Y., Vestergaard, M., Takagi, M., 2010. Biomimetic Microdroplet Membrane Interface: Detection of the Lateral Localization of Amyloid Beta Peptides. J. Phys. Chem. Lett. 1, 170–173. https://doi.org/10.1021/jz900106z

Huang, C., Lin, C., Haataja, L., Gurlo, T., Butler, A.E., Rizza, R.A., Butler, P.C., 2007. High Expression Rates of Human Islet Amyloid Polypeptide Induce Endoplasmic Reticulum Stress–Mediated β-Cell Apoptosis, a Characteristic of Humans With Type 2 but Not Type 1 Diabetes. Diabetes 56, 2016–2027. https://doi.org/10.2337/db07-0197

Jacquemyn, J., Cascalho, A., Goodchild, R.E., 2017. The ins and outs of endoplasmic reticulum - controlled lipid biosynthesis. EMBO Rep 18, 1905–1921. https://doi.org/10.15252/embr.201643426

Jang, Y., Kim, M., Hwang, S.W., 2020. Molecular mechanisms underlying the actions of

arachidonic acid-derived prostaglandins on peripheral nociception. J Neuroinflammation 17, 30. https://doi.org/10.1186/s12974-020-1703-1

Jimenez, A.J., Maiuri, P., Lafaurie-Janvore, J., Divoux, S., Piel, M., Perez, F., 2014. ESCRT Machinery Is Required for Plasma Membrane Repair. Science 343, 1247136. https://doi.org/10.1126/science.1247136

John, K., Schreiber, S., Kubelt, J., Herrmann, A., Müller, P., 2002. Transbilayer Movement of Phospholipids at the Main Phase Transition of Lipid Membranes: Implications for Rapid Flip-Flop in Biological Membranes. Biophysical Journal 83, 3315–3323. https://doi.org/10.1016/S0006-3495(02)75332-0

Kamal-Eldin, A., Gorgen, S., Pettersson, J., Lampi, A.-M., 2000. Normal-phase high-performance liquid chromatography of tocopherols and tocotrienols Comparison of different chromatographic columns. J. Chromatogr. A 217–227.

Kim, M., Sisco, N.J., Hilton, J.K., Montano, C.M., Castro, M.A., Cherry, B.R., Levitus, M., Van Horn, W.D., 2020. Evidence that the TRPV1 S1-S4 membrane domain contributes to thermosensing. Nat Commun 11, 4169. https://doi.org/10.1038/s41467-020-18026-2

Kimura, Y., Asa, M., Urano, Y., Saito, Y., Nishikawa, K., Noguchi, N., 2018. Tocopherol suppresses 24(S)-hydroxycholesterol-induced cell death via inhibition of CaMKII phosphorylation. Biochimie 153, 203–209. https://doi.org/10.1016/j.biochi.2018.07.004

King, C., Sengupta, P., Seo, A.Y., Lippincott-Schwartz, J., 2020. ER membranes exhibit phase behavior at sites of organelle contact. Proc. Natl. Acad. Sci. U.S.A. 117, 7225–7235. https://doi.org/10.1073/pnas.1910854117

Ko Sugahara, Naofumi Shimokawa, Masahiro Takagi, 2017. Thermal Stability of Phase-Separated Domains in Multicomponent Lipid Membranes with Local Anesthetics. Membranes 7, 33–47. https://doi.org/10.3390/membranes7030033

Korshavn, K.J., Satriano, C., Lin, Y., Zhang, R., Dulchavsky, M., Bhunia, A., Ivanova, M.I., Lee, Y.-H., La Rosa, C., Lim, M.H., Ramamoorthy, A., 2017. Reduced Lipid Bilayer Thickness Regulates the Aggregation and Cytotoxicity of Amyloid-β. Journal of Biological Chemistry 292, 4638–4650. https://doi.org/10.1074/jbc.M116.764092

Levental, K.R., Malmberg, E., Symons, J.L., Fan, Y.-Y., Chapkin, R.S., Ernst, R., Levental, I., 2020. Lipidomic and biophysical homeostasis of mammalian membranes counteracts dietary lipid perturbations to maintain cellular fitness. Nat Commun 11, 1339–1351. https://doi.org/10.1038/s41467-020-15203-1

Lombard, J., 2014. Once upon a time the cell membranes: 175 years of cell boundary research. Biol Direct 9, 32. https://doi.org/10.1186/s13062-014-0032-7

Mangialasche, F., Kivipelto, M., Mecocci, P., Rizzuto, D., Palmer, K., Winblad, B., Fratiglioni, L., 2010. High Plasma Levels of Vitamin E Forms and Reduced Alzheimer's Disease Risk in Advanced Age. JAD 20, 1029–1037. https://doi.org/10.3233/JAD-2010-091450

Mangialasche, F., Xu, W., Kivipelto, M., Costanzi, E., Ercolani, S., Pigliautile, M., Cecchetti, R., Baglioni, M., Simmons, A., Soininen, H., Tsolaki, M., Kloszewska, I., Vellas, B., Lovestone, S., Mecocci, P., 2012. Tocopherols and tocotrienols plasma levels are associated with cognitive impairment. Neurobiology of Aging 33, 2282–2290. https://doi.org/10.1016/j.neurobiolaging.2011.11.019

Meirer, K., Steinhilber, D., Proschak, E., 2014. Inhibitors of the Arachidonic Acid Cascade: Interfering with Multiple Pathways. Basic Clin Pharmacol Toxicol 114, 83–91. https://doi.org/10.1111/bcpt.12134

Melo van Lent, D., Egert, S., Wolfsgruber, S., Kleineidam, L., Weinhold, L., Wagner-Thelen, H., Maier, W., Jessen, F., Ramirez, A., Schmid, M., Scherer, M., Riedel-Heller, S.G., Wagner, M., 2021. Eicosapentaenoic Acid Is Associated with Decreased Incidence of Alzheimer's Dementia in the Oldest Old. Nutrients 13, 461–476. https://doi.org/10.3390/nu13020461

Morita, M., Hamada, T., Tendo, Y., Hata, T., Vestergaard, M.C., Takagi, M., 2012. Selective localization of Alzheimer's amyloid beta in membrane lateral compartments. Soft Matter 8, 2816–2819. https://doi.org/10.1039/c2sm07185a

Moskowitz, N., Andrés, A., Silva, W., Shapiro, L., Schook, W., Puszkin, S., 1985. Calcium-dependent binding of calmodulin to phospholipase A2 subunits induces enzymatic activation. Archives of Biochemistry and Biophysics 241, 413–417. https://doi.org/10.1016/0003-9861(85)90564-8

Muddana, H.S., Chiang, H.H., Butler, P.J., 2012. Tuning Membrane Phase Separation Using Nonlipid Amphiphiles. Biophysical Journal 102, 489–497. https://doi.org/10.1016/j.bpj.2011.12.033

Nakagawa, T., Zhu, H., Morishima, N., Li, E., Xu, J., Yankner, B.A., Yuan, J., 2000. Caspase-12 mediates endoplasmic- reticulum-specific apoptosis and cytotoxicity by amyloid-b 403, 98–103.

Nakazawa, T., Miyanoki, Y., Urano, Y., Uehara, M., Saito, Y., Noguchi, N., 2017. Effect of vitamin E on 24(S)-hydroxycholesterol-induced necroptosis-like cell death and apoptosis. The Journal of Steroid Biochemistry and Molecular Biology 169, 69–76. https://doi.org/10.1016/j.jsbmb.2016.03.003

Neunert, G., Tomaszewska-Gras, J., Siejak, P., Pietralik, Z., Kozak, M., Polewski, K., 2018. Disruptive effect of tocopherol oxalate on DPPC liposome structure: DSC, SAXS,

and fluorescence anisotropy studies. Chemistry and Physics of Lipids 216, 104–113. https://doi.org/10.1016/j.chemphyslip.2018.10.001

Nieto-Garai, J.A., Lorizate, M., Contreras, F.-X., 2022. Shedding light on membrane rafts structure and dynamics in living cells. Biochimica et Biophysica Acta (BBA) - Biomembranes 1864, 183813. https://doi.org/10.1016/j.bbamem.2021.183813

Nishida, Y., Ito, S., Ohtsuki, S., Yamamoto, N., Takahashi, T., Iwata, N., Jishage, K., Yamada, H., Sasaguri, H., Yokota, S., Piao, W., Tomimitsu, H., Saido, T.C., Yanagisawa, K., Terasaki, T., Mizusawa, H., Yokota, T., 2009. Depletion of Vitamin E Increases Amyloid β Accumulation by Decreasing Its Clearances from Brain and Blood in a Mouse Model of Alzheimer Disease. Journal of Biological Chemistry 284, 33400–33408. https://doi.org/10.1074/jbc.M109.054056

Parton, R.G., Simons, K., 1995. Digging into Caveolae. Science 269, 1398–1399. https://doi.org/10.1126/science.7660120

Phan, H.T.T., Vestergaard, M.C., Baek, K., Shimokawa, N., Takagi, M., 2014. Localization of amyloid beta (Aβ1-42) protofibrils in membrane lateral compartments: Effect of cholesterol and 7-Ketocholesterol. FEBS Letters 588, 3483–3490. https://doi.org/10.1016/j.febslet.2014.08.007

Piccolis, M., Bond, L.M., Kampmann, M., Pulimeno, P., Chitraju, C., Jayson, C.B.K., Vaites, L.P., Boland, S., Lai, Z.W., Gabriel, K.R., Elliott, S.D., Paulo, J.A., Harper, J.W., Weissman, J.S., Walther, T.C., Farese, R.V., 2019. Probing the Global Cellular Responses to Lipotoxicity Caused by Saturated Fatty Acids. Molecular Cell 74, 32-44.e8. https://doi.org/10.1016/j.molcel.2019.01.036

Promlek, T., Ishiwata-Kimata, Y., Shido, M., Sakuramoto, M., Kohno, K., Kimata, Y., 2011. Membrane aberrancy and unfolded proteins activate the endoplasmic reticulum stress sensor Ire1 in different ways. MBoC 22, 3520–3532. https://doi.org/10.1091/mbc.e11-04-0295

Puri, C., Tosoni, D., Comai, R., Rabellino, A., Segat, D., Caneva, F., Luzzi, P., Fiore, P.P.D., Tacchetti, C., 2005. Relationships between EGFR Signaling– competent and Endocytosis-competent Membrane Microdomains□D. Molecular Biology of the Cell 16, 15.

Radanović, T., Ernst, R., 2021. The Unfolded Protein Response as a Guardian of the Secretory Pathway. Cells 10, 2965. https://doi.org/10.3390/cells10112965

Rajendran, L., Simons, K., 2005. Lipid rafts and membrane dynamics. Journal of Cell Science 118, 1099–1102. https://doi.org/10.1242/jcs.01681

Risérus, U., Willett, W.C., Hu, F.B., 2009. Dietary fats and prevention of type 2 diabetes. Progress in Lipid Research 48, 44–51.

https://doi.org/10.1016/j.plipres.2008.10.002

Sano, R., Reed, J.C., 2013. ER stress-induced cell death mechanisms. Biochimica et Biophysica Acta (BBA) - Molecular Cell Research 1833, 3460–3470. https://doi.org/10.1016/j.bbamcr.2013.06.028

Schuck, S., Honsho, M., Ekroos, K., Shevchenko, A., Simons, K., 2003. Resistance of cell membranes to different detergents. Proc. Natl. Acad. Sci. U.S.A. 100, 5795–5800. https://doi.org/10.1073/pnas.0631579100

Schuhmacher, M., Grasskamp, A.T., Barahtjan, P., Wagner, N., Lombardot, B., Schuhmacher, J.S., Sala, P., Lohmann, A., Henry, I., Shevchenko, A., Coskun, Ü., Walter, A.M., Nadler, A., 2020. Live-cell lipid biochemistry reveals a role of diacylglycerol side-chain composition for cellular lipid dynamics and protein affinities. Proc. Natl. Acad. Sci. U.S.A. 117, 7729–7738. https://doi.org/10.1073/pnas.1912684117

Schwarz, D.S., Blower, M.D., 2016. The endoplasmic reticulum: structure, function and response to cellular signaling. Cell. Mol. Life Sci. 73, 79–94. https://doi.org/10.1007/s00018-015-2052-6

Sciacca, M.F.M., Kotler, S.A., Brender, J.R., Chen, J., Lee, D., Ramamoorthy, A., 2012. Two-Step Mechanism of Membrane Disruption by Aβ through Membrane Fragmentation and Pore Formation. Biophysical Journal 103, 702–710. https://doi.org/10.1016/j.bpj.2012.06.045

Sen, C.K., Khanna, S., Roy, S., 2006. Tocotrienols: Vitamin E beyond tocopherols. Life Sciences 78, 2088–2098. https://doi.org/10.1016/j.lfs.2005.12.001

Sezgin, E., Levental, I., Mayor, S., Eggeling, C., 2017. The mystery of membrane organization: composition, regulation and roles of lipid rafts. Nat Rev Mol Cell Biol 18, 361–374. https://doi.org/10.1038/nrm.2017.16

Sharma, N., Baek, K., Phan, H.T.T., Shimokawa, N., Takagi, M., 2017. Glycosyl chains and 25-hydroxycholesterol contribute to the intracellular transport of amyloid beta (Aβ-42) in Jurkat T cells. FEBS Open Bio 7, 865–876. https://doi.org/10.1002/2211-5463.12234

Shen, Y., Zhao, Z., Zhang, L., Shi, L., Shahriar, S., Chan, R.B., Di Paolo, G., Min, W., 2017. Metabolic activity induces membrane phase separation in endoplasmic reticulum. Proc Natl Acad Sci USA 114, 13394–13399. https://doi.org/10.1073/pnas.1712555114

Shimizu, M., Nakamura, H., Hirabayashi, T., Suganami, A., Tamura, Y., Murayama, T., 2008. Ser515 phosphorylation-independent regulation of cytosolic phospholipase A2α (cPLA2α) by calmodulin-dependent protein kinase: Possible interaction with

catalytic domain A of cPLA2α. Cellular Signalling 20, 815–824. https://doi.org/10.1016/j.cellsig.2007.12.016

Shimokawa, N., Mukai, R., Nagata, M., Takagi, M., 2017. Formation of modulated phases and domain rigidification in fatty acid-containing lipid membranes. Phys. Chem. Chem. Phys. 19, 13252–13263. https://doi.org/10.1039/C7CP01201B

Simons, K., Ikonen, E., 1997. Functional rafts in cell membranes 387, 4.

Singer, S.J., Nicolson, G.L., 1972. The Fluid Mosaic Model of the Structure of Cell Membranes: Cell membranes are viewed as two-dimensional solutions of oriented globular proteins and lipids. Science 175, 720–731. https://doi.org/10.1126/science.175.4023.720

Szegezdi, E., Logue, S.E., Gorman, A.M., Samali, A., 2006. Mediators of endoplasmic reticulum stress‐induced apoptosis. EMBO Rep 7, 880–885. https://doi.org/10.1038/sj.embor.7400779

Tabas, I., Ron, D., 2011. Integrating the mechanisms of apoptosis induced by endoplasmic reticulum stress. Nat Cell Biol 13, 184–190. https://doi.org/10.1038/ncb0311-184

Thibault, G., Shui, G., Kim, W., McAlister, G.C., Ismail, N., Gygi, S.P., Wenk, M.R., Ng, D.T.W., 2012. The Membrane Stress Response Buffers Lethal Effects of Lipid Disequilibrium by Reprogramming the Protein Homeostasis Network. Molecular Cell 48, 16–27. https://doi.org/10.1016/j.molcel.2012.08.016

Tian, M., Sun, Y., Kong, X., Dong, B., 2022. Revealing the Phase Separation in ER Membranes of Living Cells and Tissues by *In Situ* NIR Ratiometric Imaging. Anal. Chem. 94, 2844–2854. https://doi.org/10.1021/acs.analchem.1c04596

Umeda, T., Tomiyama, T., Sakama, N., Tanaka, S., Lambert, M.P., Klein, W.L., Mori, H., 2011. Intraneuronal amyloid β oligomers cause cell death via endoplasmic reticulum stress, endosomal/lysosomal leakage, and mitochondrial dysfunction in vivo. J. Neurosci. Res. 89, 1031–1042. https://doi.org/10.1002/jnr.22640

Urano, Y., Ho Vo, D.-K., Hirofumi, A., Noguchi, N., 2019. 24(S)-Hydroxycholesterol induces ER dysfunction-mediated unconventional cell death. Cell Death Discov. 5, 113–125. https://doi.org/10.1038/s41420-019-0192-4

van Meer, G., Voelker, D.R., Feigenson, G.W., 2008. Membrane lipids: where they are and how they behave. Nat Rev Mol Cell Biol 9, 112–124. https://doi.org/10.1038/nrm2330

van Swaay, D., deMello, A., 2013. Microfluidic methods for forming liposomes. Lab Chip 13, 752. https://doi.org/10.1039/c2lc41121k

Veatch, S.L., Keller, S.L., 2005. Seeing spots: Complex phase behavior in simple membranes. Biochimica et Biophysica Acta (BBA) - Molecular Cell Research 1746, 172–185.

https://doi.org/10.1016/j.bbamcr.2005.06.010

Veatch, S.L., Keller, S.L., 2003. Separation of Liquid Phases in Giant Vesicles of Ternary Mixtures of Phospholipids and Cholesterol. Biophysical Journal 85, 3074–3083. https://doi.org/10.1016/S0006-3495(03)74726-2

Villaseñor, R., Nonaka, H., Del Conte-Zerial, P., Kalaidzidis, Y., Zerial, M., 2015. Regulation of EGFR signal transduction by analogue-to-digital conversion in endosomes. eLife 4, e06156. https://doi.org/10.7554/eLife.06156

Vinardell, M.P., Mitjans, M., 2008. Alternative Methods for Eye and Skin Irritation Tests: An Overview. Journal of Pharmaceutical Sciences 97, 46–59. https://doi.org/10.1002/jps.21088

Volmer, R., K. van der Ploeg, Ron, D., 2013. Membrane lipid saturation activates endoplasmic reticulum unfolded protein response transducers through their transmembrane domains. Proceedings of the National Academy of Sciences 110, 4628–4633. https://doi.org/10.1073/pnas.1217611110

Wiggins, P., Phillips, R., 2004. Analytic models for mechanotransduction: Gating a mechanosensitive channel. Proceedings of the National Academy of Sciences 101, 4071–4076. https://doi.org/10.1073/pnas.0307804101

Wilhelmus, K.R., 2001. The Draize Eye Test. Survey of Ophthalmology 45, 493–515. https://doi.org/10.1016/S0039-6257(01)00211-9

Wilson, S.L., Ahearne, M., Hopkinson, A., 2015. An overview of current techniques for ocular toxicity testing. Toxicology 327, 32–46. https://doi.org/10.1016/j.tox.2014.11.003

Wongsirojkul, N., Masuta, A., Shimokawa, N., Takagi, M., 2022. Control of Line Tension at Phase-Separated Lipid Domain Boundaries: Monounsaturated Fatty Acids with Different Chain Lengths and Osmotic Pressure. Membranes 12, 781. https://doi.org/10.3390/membranes12080781

Wongsirojkul, N., Shimokawa, N., Opaprakasit, P., Takagi, M., Hamada, T., 2020. Osmotic-Tension-Induced Membrane Lateral Organization. Langmuir 36, 2937–2945. https://doi.org/10.1021/acs.langmuir.9b03893

Yanai, H., 2017. Effects of N-3 Polyunsaturated Fatty Acids on Dementia. J Clin Med Res 9, 1–9. https://doi.org/10.14740/jocmr2815w

Zhen, Y., Radulovic, M., Vietri, M., Stenmark, H., 2021. Sealing holes in cellular membranes. EMBO J 40. https://doi.org/10.15252/embj.2020106922

Acknowledgment

I would like to express my deepest gratitude to my supervisor Prof. Masahiro Takagi for his invaluable advice on this theme and encouragement in carrying out this study. Daily discussions with him help me acquire not only specialized knowledge about biological membranes but also the way of thinking as a scientist.

I would also like to express my sincere gratitude to Dr. Naofumi Shimokawa for his comments from a physics point of view and technical advice on experiments. His support allowed me to perform a more detailed data analysis.

I thank Prof. Noriko Noguchi and Assoc. Prof. Yasuomi Urano. They gave me important knowledge that triggered this research and kindly provided me with the reagents.

I thank lab members for their support in creating a good environment for studying.

Publication list

Journal Papers

1. Yusuke Nakatani, Naofumi Shimokawa, Yasuomi Urano, Noriko Noguchi, and Masahiro Takagi. Suppression of Amyloid-β Adsorption on Endoplasmic Reticulum Stress-Mimicking Membranes by α-Tocopherol and α-Tocotrienol. *Journal of Physical Chemistry Letters* **2022**, *13*(51), 11955-11960.

2. Yusuke Nakatani, Taichi Ito, Naofumi Shimokawa, Yuriye Mandai, Gang An, Shuichi Takase, Yoshio Tsujino, Masahiro Takagi. Surfactant-induced membrane dynamics and skin irritation (in preparation)

Presentations at academic conferences

1. Yusuke Nakatani, Taichi Ito, Naofumi Shimokawa, Yuriye Mandai, Gang An, Shuichi Takase, Yoshio Tsujino, Masahiro Takagi『The 74th Society for Biotechnology, Japan Annual meeting』October 2022 online
2. Yusuke Nakatani, Taichi Ito, Naofumi Shimokawa, Yuriye Mandai, Gang An, Shuichi Takase, Yoshio Tsujino, Masahiro Takagi「Evaluation of Surfactant-Induced Irritation by Cell Membrane Model System」『The 102nd Chemical Society of Japan Annual meeting』March 2022 online
3. Yusuke Nakatani, Naofumi Shimokawa, Yasuomi Urano, Noriko Noguchi, Masahiro Takagi, 「Effects of Vitamin E with Different Degrees of Saturation on Membrane Interactions with Amyloid β」『The 101st Chemical Society of Japan Annual meeting』March 2021 online (Poster)
4. Yusuke Nakatani, Naofumi Shimokawa, Yasuomi Urano, Noriko Noguchi, Masahiro Takagi 「Effects of Vitamin E with Different Saturation Levels on Membrane Phase Separation Formation and Amyloid β Adsorption Behavior」『Hokuriku Chemical Society of Japan』November 2020 online (Poster)
5. Yusuke Nakatani, Naofumi Shimokawa, Yasuomi Urano, Noriko Noguchi, Masahiro Takagi 「Domain formation and Aβ adsorption behavior in biomimetic membranes containing vitamin E with different hydrophobic parts」『The 14th Sympsium on Biorelevant Chemistry』September 2020 online (Poster)

Award

1. Yusuke Nakatani, November 2020, 『CSJ Kinki Poster Presentation Award 2020 For Excellent Research』,